

Submitted to Astronomical Journal

## The Chemical Composition of Two Supergiants in the Dwarf Irregular Galaxy WLM

Kim A. Venn

*Macalester College, Saint Paul, MN, 55105; venn@macalester.edu  
University of Minnesota, 116 Church Street S.E., Minneapolis, MN, 55455*

Eline Tolstoy

*Kapteyn Institute, University of Groningen, PO Box 800, 9700AV Groningen, the  
Netherlands; etolstoy@astro.rug.nl*

Andreas Kaufer

*European Southern Observatory, Alonso de Cordova 3107, Santiago 19, Chile;  
akauffer@eso.org*

Evan D. Skillman

*Department of Astronomy, University of Minnesota, 116 Church Street S.E., Minneapolis,  
MN, 55455; skillman@astro.umn.edu*

Sonya M. Clarkson

*Macalester College, Saint Paul, MN, 55105*

Stephen J. Smartt

*Institute of Astronomy, University of Cambridge, Madingley Road, Cambridge, CB3 0HA,  
UK; sjs@ast.cam.ac.uk*

Danny J. Lennon

*Isaac Newton Group of Telescopes (ING), Santa Cruz de La Palma, Canary Islands,  
E-38700, Spain; djl@ing.iac.es*

and

Rolf P. Kudritzki

*Institute for Astronomy, University of Hawaii, 2680 Woodlawn Drive, Honolulu, 95822;  
kud@ifh.hawaii.edu*

## ABSTRACT

The chemical composition of two stars in WLM have been determined from high quality UVES data obtained at the VLT UT2<sup>1</sup>. The model atmospheres analysis shows that they have the same metallicity,  $[\text{Fe}/\text{H}] = -0.38 \pm 0.20$  ( $\pm 0.29$ )<sup>2</sup>. Reliable magnesium abundances are determined from several lines of two ionization states in both stars resulting in  $[\text{Mg}/\text{Fe}] = -0.24 \pm 0.16$  ( $\pm 0.28$ ). This result suggests that the  $[\alpha(\text{Mg})/\text{Fe}]$  ratio in WLM may be suppressed relative to solar abundances (also supported by differential abundances relative to similar stars in NGC 6822 and the SMC). The absolute Mg abundance,  $[\text{Mg}/\text{H}] = -0.62$  is high relative to what is expected from the nebulae though, where two independent spectroscopic analyses of the H II regions in WLM yield  $[\text{O}/\text{H}] = -0.89$ . Intriguingly, the oxygen abundance determined from the O I  $\lambda 6158$  feature in one WLM star is  $[\text{O}/\text{H}] = -0.21 \pm 0.10$  ( $\pm 0.05$ ), corresponding to five times higher than the nebular oxygen abundance. This is the first time that a significant difference between stellar and nebular oxygen abundances has been found, and presently, there is no simple explanation for this difference. The two stars are massive supergiants with distances that clearly place them in WLM. They are young ( $\leq 10$  Myr) and should have a similar composition to the ISM. Additionally, differential abundances suggest that the O/Fe ratio in the WLM star is consistent with similar stars in NGC6822 and the SMC, galaxies where the average stellar oxygen abundances are in excellent agreement with the nebular results. If the stellar abundances reflect the true composition of WLM, then this galaxy lies well above the metallicity-luminosity relationship for dwarf irregular galaxies. It also suggests that WLM is more chemically evolved than currently interpreted from its color-magnitude diagram. The similarities between the stars in WLM and NGC6822 suggest that these two galaxies may have had similar star formation histories.

---

<sup>1</sup>Based on observations collected at the European Southern Observatory, proposal number 65.N-0375

<sup>2</sup>In this paper, we adopt the standard notation  $[X/\text{H}] = \log(X/\text{H}) - \log(X/\text{H})_{\odot}$ . Also, abundances shall be reported with two uncertainties: the first is the line-to-line scatter, and the second (in parentheses and italics) is an *estimate* of the systematic error due to uncertainties in the atmospheric parameters.

*Subject headings:* galaxies: abundances, dwarf galaxies, individual (WLM) stars:  
abundances

## 1. Introduction

The evolution of the chemical abundances in a galaxy is intimately linked to its star formation history (Tinsley 1979). Different elements are produced during the evolution of stars of different masses, and over a range of timescales. If the star formation in a galaxy proceeds by a series of bursts, as suggested for dwarf galaxies (c.f., Matteucci & Tosi 1985, and reviews by Hodge 1989 and Mateo 1998), rather than smooth, approximately constant star formation that characterizes the evolution of galactic disks (e.g., Matteucci & Greggio 1986, Edvardsson et al. 1993, Chiappini et al. 1997) then this should lead to clear differences in the evolution of the chemical abundances. One ratio of particular importance is the  $\alpha/\text{Fe}$  ratio. Oxygen is produced primarily in high-mass stars of negligible lifetimes and ejected by SNe II, while iron is produced in both SNe II and SNe Ia. Stars that form shortly after the interstellar medium has been enriched by SNe II may have enriched  $\alpha/\text{Fe}$  ratios, while those that form sometime after the SNe Ia contribute will have lower  $\alpha/\text{Fe}$  ratios. The timescale for changes in the  $\alpha/\text{Fe}$  ratio depends not only on the SFH, but also on the IMF, the SNe Ia timescale, and the timescales for mixing the SNe Ia and SNe II products back into the interstellar medium. Gilmore and Wyse (1991) demonstrated the expected differences in  $\alpha/\text{Fe}$  ratios in galaxies with different star formation histories. Most notably they write “We emphasize that there is nothing special or universal about solar element ratios, and that one should not expect the solar neighborhood situation to be reproduced in any other environment which has had a different star formation history.” The analysis of bright nebular emission lines of H II regions (and some PN) has been the most frequent approach to modeling the chemical evolution of galaxies to date (see Pagel 1997), and yet only a limited number of elements can be examined and quantified when using this approach. In particular, iron-group abundances, and thus the  $\alpha/\text{Fe}$  ratios, are either not possible or carry significant uncertainties from nebular analyses alone. Supergiant stars, however, have both  $\alpha$  and iron-group element absorption lines in their spectra, and it is possible to obtain a reliable  $\alpha/\text{Fe}$  ratio from these stars<sup>3</sup>

---

<sup>3</sup>The most reliable ratios, of particular  $\alpha$  and Fe-group elements, varies depending on the temperature of the supergiant (blue versus red) analysed. In the analysis of A-type supergiants, O I Mg I and Mg II usually provide the most reliable  $\alpha$  element abundances, while Cr II and Fe II provide the best Fe-group results.

Imaging of dwarf galaxies in the Local Group show a wide variety of star formation histories (Grebel 1997, Mateo 1998). Measuring  $\alpha/\text{Fe}$  ratios in stars of various ages provides an ideal way to test these star formation histories and constrain the chemical evolution of these galaxies. This is possible for the closest galaxies from detailed analyses of their red giants, i.e., the Magellanic Clouds (Hill et al. 2003) and Galactic dSph galaxies (Bonifacio et al. 2000, Shetrone, Cote, & Sargent 2001, Shetrone et al. 2003, Tolstoy et al. 2003). Some dwarf irregular galaxies appear to have undergone bursts of star formation during their histories and thus should show a variety of  $\alpha/\text{Fe}$  ratios throughout their evolution, but they are too distant for detailed analysis of their red giant branch (=RGB, stars that can sample ages  $>1$  Gyr). It is possible to observe and analyse the spectra of their bright, young massive stars though, since they continue to form stars today. These stars will reflect the *integrated* star formation history and chemical evolution in their  $\alpha/\text{Fe}$  abundances, and yet Gilmore and Wyse (1991) predict that this ratio could vary significantly from galaxy to galaxy.

While dwarf galaxies are the most common type of galaxy in the Local Group (c.f., van den Bergh 2000), the dwarf spheroidal galaxies are (almost) all located near the large mass galaxies, which suggests that their environment may be related to their morphology and possibly star formation history (van den Bergh 1994). On the other hand, dwarf irregular galaxies tend to be more isolated systems found on the outskirts of the Local Group. Nebular analyses suggest that the low luminosity dwarf irregular galaxies are very metal-poor ( $\sim 1/20$  solar, Skillman et al. 1989a,b), suggesting that they have undergone relatively little chemical evolution. These objects may be more similar to the protogalactic fragments at the time of Galaxy formation in hierarchical merging models; low mass, gas rich, and metal-poor.

WLM (DDO221, UGCA444) is an isolated dwarf irregular galaxy and its star formation history has been studied in detail with HST STIS imaging by Rejkuba et al. (2000) and HST WFPC2 imaging by Dolphin (2000), building on the ground-based studies by Minniti & Zijlstra (1997, hereafter MZ97) and Ferraro et al. (1989). Rejkuba et al.'s detection of the horizontal branch confirmed the distance modulus of WLM at  $(m - M)_0 = 24.95 \pm 0.13$ , the foreground reddening at  $E(V-I) = 0.03$ , and the presence of an ancient population. Their distance  $D = 0.98 \pm 0.06$  Mpc is within  $1\sigma$  of the  $D_{WLM} = 0.95$  summarized by van den Bergh (1994, 2000), which includes a revision of the Cepheid distance originally found by Sandage & Carlson (1985). Dolphin used the CMD to examine the star formation and chemical enrichment history of WLM, finding that more than half the stars in WLM formed over 9 Gyr ago. The star formation rate has gradually decreased since then, with a recent increase that is concentrated in the bar of the galaxy. The metal enrichment appears to show a gradual increase from  $[\text{Fe}/\text{H}] \leq -2$  over 12 Gyr ago, reaching a current value near  $-1$  dex. This low present-day value is consistent with the published nebular abundance,  $12+\log(\text{O}/\text{H}) = 7.77 \pm 0.17$  based on three H II regions (Hodge & Miller 1995, hereafter

HM95; Skillman et al. 1989a), or an abundance relative to solar<sup>4</sup> of  $[O/H] = -0.89$ . WLM lies well above the plane of the Local Group and is fairly isolated, thus MZ97 argue, based on its distance to IC1613, that it could not have suffered a major encounter within the past Gyr to initiate its current star formation activity. However, since then the Cetus dwarf spheroidal galaxy has been discovered (Whiting, Hau, & Irwin 1999), which is located much closer to WLM than IC1613. Another possibility is if the one globular cluster in WLM (see also Hodge et al. 1999) passed near the center of the galaxy and caused a disruption, but the globular cluster space velocities are not known.

The distance to WLM puts the tip of the red giant branch at  $V \sim 22$ , which is out of reach for detailed chemical abundance analyses of its RGB population. However, there are bright blue supergiants in WLM’s central star forming region with  $V \sim 18$ . These young, massive stars sample the current metallicity in the galaxy (thus the integrated metal enrichment over its lifetime), and provide valuable end-point abundances, particularly for the iron-group, as well as for the s-process; but they do not provide information on the evolution of these abundances (as in RGB analyses). They can also provide a check on the accuracy of the  $\alpha$  element abundances from nebular spectroscopy. Model atmospheres analyses of the massive stars in Orion (Cunha & Lambert 1994), the Large Magellanic Cloud (LMC; Hill 1999, Hill et al. 1995, Rolleston et al. 2002, Korn et al. 2002), the Small Magellanic Cloud (SMC; Venn 1999, Hill 1997, Rolleston et al. 2003), the Andromeda galaxy (M31; Venn et al. 2000, Trundle et al. 2002), and the dwarf irregular galaxy NGC6822 (Venn et al. 2001), have all determined stellar oxygen abundances in excellent agreement with the nebular results. In this paper, we present the first stellar abundances in WLM.

## 2. Observations & Reductions

Spectra for two A-type supergiants and one B-type supergiant in WLM were taken at the VLT-UT2 with UVES (Dekker et al. 2000) between August 20–22, 2000 (Table 1). 60-minute exposures of each star were made in (mostly) sub-arcsecond seeing conditions through a 1.0-arcsec slit. On-chip binning (2x2) was used at readout, yielding  $R \sim 32,000$ , or  $R \sim 20,000$  per 3 pixel resolution element. A combined S/N ratio  $\sim 30$  per pixel, or S/N  $\sim 50$  per resolution element, was attained after coaddition. Two dichroic settings (390/564 and non-standard 390/840) were used with standard calibrations and pipeline reduced. The pipeline reduction (Balester et al. 2000) includes bias and interorder background subtraction,

---

<sup>4</sup>Note that this ratio is based on a solar oxygen abundance of  $12 + \log(O/H) = 8.66$  from Asplund (2003, consistent with Allende-Prieto et al. 2001).

flatfield correction, optimal extraction (with cosmic ray rejection) above the sky level, and the wavelength calibration. The wavelength range spanned  $3800 \text{ \AA} \leq W_\lambda \leq 10250 \text{ \AA}$ , with gaps near  $4600 \text{ \AA}$ ,  $5600 \text{ \AA}$ , and from  $6650 - 8470 \text{ \AA}$ .

Targets were selected from photometric BVI colors (from archival NTT imaging) and from low resolution spectroscopy (from WHT-ISIS and ESO 3.6m EFOSC spectroscopy by D.J. Lennon and S.J. Smartt, and FORS2 spectroscopy by T. Szeifert). We selected the brightest ( $V < 18.5$ ), apparently isolated stars, with colors ranging from  $-0.3 \leq (B-V)_o \leq 0.6$ . The six brightest stars from the original target list are in Table 2. Unfortunately, further analysis of the UVES spectrum of the early B-type star WLM-35 is not possible because of missing Si III lines, needed for the effective temperature determination, in the dichroic gap near  $4600 \text{ \AA}$ . The locations of these stars in WLM can be seen in Fig. 1 (coordinates available in Sandage & Carlson 1985).

The two stars analysed here are WLM-15 and WLM-31. WLM-15 proved to be that of a normal, isolated A5 Ib supergiant, with a radial velocity consistent with WLM membership (Table 2). WLM-31 is a blend of a normal mid-A supergiant and a foreground red giant. The red giant spectrum has been subtracted for this analysis (discussed further below). This has been possible partially because it contributes very little light in the blue compared to the A-type supergiant and because its radial velocity,  $\sim 0 \text{ km s}^{-1}$  (which is consistent with the Galaxy halo stars at WLM’s Galactic coordinates), is well offset from the A-supergiant in WLM ( $-117 \text{ km s}^{-1}$ ).

Finally, we mention that spectra of hot, rapidly-rotating stars were taken as telluric divisors, but not used. The S/N in our WLM spectra was too low in the red spectral regions where the telluric divisors would have been useful (e.g., N I 8200 lines) for further analysis. There were no telluric lines near the Mg II 7880 features used in this analysis.

### 3. Atmospheric Analyses

The WLM A-supergiants have been analysed using ATLAS9 (hydrostatic, line-blanketed, plane parallel) model atmospheres (Kurucz 1979, 1888). These atmospheres have been shown to be appropriate for the photospheric analysis of lower luminosity A-supergiants (Przybilla 2002), and have been successfully used for the photospheric analysis of stars in the Galaxy, the Magellanic Clouds, and M31 (Venn 1995a,b, 1999; Luck et al. 1998; Venn et al. 2000; Przybilla 2002). A-type supergiants require a tailored analysis where only weak spectral lines (that typically form deep in the photosphere) are included. In this analysis, weak lines are defined as those where a change in microturbulence ( $\xi$ ),  $\Delta\xi = \pm 1 \text{ km s}^{-1}$ , yields a change

in abundance of  $\log(X/H) \leq 0.1$ . Typically, this was found to be  $W_\lambda \leq 160 \text{ m}\text{\AA}$ . Using weak lines exclusively also helps to avoid uncertainties in the model atmospheres analysis due to neglected NLTE and spherical extension effects in the atmospheric structure, as well as NLTE and  $\xi$  effects in the line formation calculations.

The critical spectral features used to determine the model atmosphere parameters (effective temperature,  $T_{\text{eff}}$ , and gravity) are the wings of the  $H\gamma$  line (see Fig. 2) and ionization equilibrium of Mg I and Mg II (discussed below for each star individually). A locus of  $T_{\text{eff}}$ -gravity pairs that reproduce the Balmer line and Mg ionization equilibrium are shown in Fig. 3. NLTE calculations are included for Mg using the model atom developed by Gigas (1988) and a system of programs first developed by W. Steenbock at Kiel University and further developed and upgraded by M. Lemke (now associated with the Dr. Remeis-Sternwarte, Bamberg). The results from this model are in very good agreement with the more recent Mg model developed by Przybilla et al. (2001a). The NLTE corrections for Mg are quite small; for both stars, the Mg II corrections are  $\leq 0.03$  dex, and for Mg I they average  $-0.11$  dex (with a range from  $-0.02$  to  $-0.16$  dex). Ionization equilibrium of Fe I and Fe II is also shown in Fig. 3, but only used as a check since NLTE effects may be important for Fe I (e.g., Boyarchuk et al. 1985, Gigas 1986). Fe II NLTE effects are negligible (Becker 1998).

Microturbulence has been found by examining the line abundances of Fe II, Ti II, Cr II (and Fe I), and require no relationship with equivalent width. The results from Fe I were consistently lower, although allowing for an uncertainty in  $\Delta\xi$  of  $\pm 1 \text{ km s}^{-1}$  brings the results from the different species into excellent agreement. Considering the weak line nature of this analysis, a single value for  $\xi$  was adopted for each star.

The atmospheric parameters determined for both stars are listed in Table 4. The uncertainties in  $T_{\text{eff}}$  for WLM-15,  $\Delta T_{\text{eff}} = \pm 200 \text{ K}$ , is estimated from the range where  $\log(\text{Mg II}) = \log(\text{Mg I}) \pm 0.2$  when holding gravity fixed. This range allows for uncertainties in equivalent width measurements, atomic data, and uncertainties in the NLTE calculations. The uncertainty in  $T_{\text{eff}}$  for WLM-31 is larger,  $\Delta T_{\text{eff}} = \pm 300 \text{ K}$ , because only one weak line of Mg II is available for the analysis (we consider a significant uncertainty on its equivalent width measurement  $W_\lambda = 25 \pm 10 \text{ m}\text{\AA}$ ), and the measurements of the Mg I  $\lambda 5180$  lines are less certain (see the discussion on recovering the spectrum of WLM-31 from a blend with a foreground red giant, Section 3.1). The uncertainties in gravity,  $\Delta \log g = \pm 0.1$ , are estimated from the range in the  $H\gamma$  profile fits while holding  $T_{\text{eff}}$  fixed for both stars.

### 3.1. Recovering the Intrinsic Spectrum of WLM 31

WLM-31 shows sharp and narrow Mg I 5180 lines at the radial velocity offset of the WLM galaxy, but also strong and broad Mg Ib lines at the Galactic rest wavelengths. It appears to be an A-supergiant in WLM, combined with a foreground red giant.

There are no HST images for WLM-31. Examination of the FORS images in B, V, and I of WLM (with seeing estimates of 0.75, 0.81, 1.07 arcseconds, respectively) reveal that this object is sharp in the I image, yet in the B (and possibly V) image, where the seeing estimate is the lowest and the color difference between the two stars would be the highest, there is a marginal asymmetry to the northeast. A  $\sim 40\%$  contribution by the RGB star to the V-band continuum in the UVES spectrum of WLM-31 (discussed in the next section), corresponds to a difference in magnitude of  $\Delta V \leq 0.5$ , within  $\sim 0.7''$ .

Since the radial velocities and spectral types of these two stars are so different, we have attempted to recover and analyse the A-supergiant spectrum in WLM; see Fig. 4. As a first step, the normalized UVES spectrum of WLM-15 was combined with that of a variety of red giants (RGB UVES spectra from Shetrone et al. 2003). Combining WLM-15 with a red giant near 4100 K (e.g., Fornax-M12) reproduces the 5200 Å spectral region quite well if the RGB spectrum is weighted at 40%. The same was true near 4900 Å if the RGB spectrum was weighted at 25%. As a second step, the surface flux for a normal A-type supergiant (WLM-15 parameters) was compared to that of a metal-poor red giant ( $[\text{Fe}/\text{H}] = -1.5$ ,  $T_{\text{eff}}=4250$  K,  $\log g = 1.0$ ) and a metal-poor red dwarf ( $[\text{Fe}/\text{H}]=-1.5$ ,  $T_{\text{eff}}=4250$  K,  $\log g = 4.0$ ) using Kurucz (1993) models<sup>5</sup>. If the red giant flux contributes 25% near 4900 Å, then the Kurucz fluxes reproduce our estimated flux ratio at 5200 Å (as 37%). This estimate is the same for the red dwarf (since the continuum level is dominated by temperature). The Kurucz fluxes can also be used to estimate the contribution from the RGB stars to the A-supergiant’s continuum below 4900 Å.

The line list for WLM-31 was taken from our analysis of WLM-15 (since their spectra are quite similar). Equivalent widths were measured, then scaled depending on their wavelength; contamination by the RGB star has been estimated per wavelength by comparing Kurucz (1993) model atmospheres (as described above). The scaling used for the equivalent widths was 37%, 25%, 20%, 15%, 9%, and 2% at 5200 Å, 4900 Å, 4600 Å, 4400 Å, 4200 Å, and 4000 Å, respectively, based on the Kurucz fluxes, with linear interpolation used for wavelengths between these points. This scaling law varies slightly for Kurucz models with  $\Delta T_{\text{eff}} = \pm 250$  K but does not affect our WLM-31 elemental abundances ( $\Delta \log(X/\text{H})$ )

---

<sup>5</sup>Available from stsci.edu at ftp.stsci.edu/cdbs/cdbs2/grid/k93models/

$\leq 0.02$  dex). Spectral lines above  $5200 \text{ \AA}$  were not used since the RGB star begins to dominate the spectrum, washing out the weak spectral lines in the A-supergiant and making the continuum corrections more uncertain. When the abundances were calculated, the results from blue versus red absorption lines were in excellent agreement after this scaling, suggesting that we have sufficiently recovered the A-supergiant spectrum. However, several lines observed in WLM-15 were not recovered in WLM-31. Very weak lines were not recovered because the S/N for the WLM-31 spectrum is slightly lower, and some stronger lines were not recovered because WLM-31 is slightly cooler such that changing  $\xi$  by  $1 \text{ km s}^{-1}$  changed  $\log(X/H)$  by  $\geq 0.1$  dex (the definition for a weak line to be used in this analysis). As a final step, each individual absorption line used in the WLM-31 analysis was reviewed, and any lines that were clearly contaminated by a strong RGB line were discarded (of course, the RGB contaminating lines were from different elements and transitions because of the radial velocity offset). Thus, the set of line measurements listed in Table 3 are considered to be the most reliable in the WLM-31 spectrum.

Clearly the abundances from WLM-31 should be viewed with caution considering the difficulties deconvolving the two stars (particularly not being able to clearly analyse the RGB contaminant itself because we do not know its actual atmospheric parameters). Nevertheless, the spectral analysis of this star is remarkably consistent between the blue and red spectral lines that we have carefully selected in the spectrum, and from species to species (below).

### 3.2. WLM Membership

Because it is important to be as certain as possible that these stars are members of WLM, the atmospheric parameters determined above are used here to derive a spectroscopic distance. Even though these distances are not very accurate, we do this as a consistency check and to ensure that they are not foreground (post-AGB?) stars. The calculation is straightforward for the isolated star, WLM-15, but difficult for the blended star WLM-31 without knowing the difference in magnitude between the A-supergiant and the foreground red giant.

For WLM-15, we adopt  $12 M_{\odot}$  as a reasonable mass estimate from its atmospheric parameters and standard stellar evolution tracks (e.g., Lejeune & Schaerer 2001). Low foreground reddening is consistently found to WLM (see discussion by Rejkuba et al. 2000). Adopting  $E(B-V) = 0.03$ , and zero bolometric correction, the distance to WLM-15 is  $\sim 850$  kpc. The mass estimate and gravity determination are the most critical factors in this calculation; allowing mass to vary by  $\pm 6 M_{\odot}$  or gravity to vary by  $\mp 0.2$  dex can change the distance by  $\pm 200$  kpc. All other parameters (e.g., temperature estimate, bolometric correction, and in-

ternal reddening up to  $A_v=0.4$ ) have much smaller effects. This stellar distance is in excellent agreement with that summarized by van den Bergh (1994, 2000) of  $D_{WLM} = 0.95$  Mpc.

The distance to WLM-31 is much less certain because the A-supergiant in WLM is blended with a foreground red giant, and we cannot be as certain of its physical properties. As an estimate, if the red giant contributes 40% of the light in the V-band (see Section 3.1), then the magnitude of the remaining A-supergiant is  $\sim 0.5$  mag fainter, or  $V \sim 18.9$ . Adopting the same mass and reddening used for WLM-15, since they have similar atmospheric parameters, then the distance is  $\sim 1200$  kpc. This is in fair agreement with  $D_{WLM}$ . However, if WLM-31 is really 0.8 mag fainter than WLM-15, then either WLM-31 must have higher (internal) foreground reddening or a lower mass. For reddening,  $\Delta A_v \sim 0.7$  is much higher than inferred from the CMD analyses; e.g., MZ97 set an upper limit to the differential reddening at 0.1 mag by comparing the RGB and blue main sequence on both sides of WLM. However, Skillman et al. (1989) suggest an upper limit to the total extinction of  $A_B \leq 0.4$  to 0.5, and Hodge & Miller (1995) find  $E(B-V) = 0.1 \pm 0.1$  for two H II regions in WLM, or  $A_v \leq 0.6$ . These high values could bring WLM-31 into agreement with WLM-15 (which would need to have zero reddening then). On the other hand, if WLM-31 had a mass near  $6 M_\odot$ , instead of  $12 M_\odot$  adopted for WLM-15, and given their similar atmospheric parameters, then this would imply a difference of  $\sim 0.3$  in luminosity, or  $\sim 0.8$  mag! The new distance modulus ( $\sim 900$  kpc) would be in excellent agreement with  $D_{WLM}$  for both stars. Such a low mass is unlikely for the atmospheric parameters derived for this star though, even if the parameters for this star are less certain. An intermediate solution would be more satisfactory, e.g., if WLM-31 has a mass near  $9 M_\odot$  and a slightly higher gravity near  $\log g = 1.8$  (or only  $1.5 \sigma_{\log g}$ ), then the distance modulus would be in good agreement ( $\sim 900$  kpc) and these values are within reasonable uncertainties in this analysis. Without being able to quantify the foreground red giant more accurately, then we will not speculate further on the distance to WLM-31.

We have also looked for the nebular/interstellar features in the WLM spectrum, such as interstellar NaD lines from WLM, which would be a direct confirmation of the membership of these stars. No NaD (nor Ca H/K) lines at the WLM H I radial velocity were found, however this is consistent with an upper-limit to the Na I interstellar abundance. Assuming a limiting  $W_\lambda$  of  $30 \text{ m}\text{\AA}$ , and estimating a hydrogen column density from its H I 21-cm flux,  $300 \text{ Jy km s}^{-1}$  (Huchtmeier & Richter 1986) suggests that  $N(\text{Na I})/N(\text{H I}) \leq 4 \times 10^{-9}$ . This upper limit falls just above the Galactic relationship determined by Hobbs (1974), thus our non-detection of NaD does *not* suggest that these are foreground objects. However, the raw 2-D spectral images of WLM-15 *do* show diffuse H $\alpha$  emission centered around the H I radial velocity of WLM ( $-123 \pm 3 \text{ km s}^{-1}$ , Huchtmeier & Richter 1986). The diffuse emission is nearly symmetric on either side of the stellar spectrum. The FWHM is  $57 \text{ km s}^{-1}$ , corresponding to a ( $1\sigma$ ) velocity dispersion of  $24 \text{ km s}^{-1}$ . This is in excellent agreement with

the thermal velocity ( $22 \text{ km s}^{-1}$ ) of the warm interstellar medium (assuming a temperature of 10,000 K). Thus, diffuse  $\text{H}\alpha$  emission from the WLM dwarf galaxy is detected in the spectrum of WLM-15.

Finally, the possibility that the A-supergiants are foreground post-AGB stars must be considered. Post-AGB stars can resemble A-type supergiants (e.g., Venn et al. 1998), typically with low iron-group abundances, higher abundances for elements that do not condense into dust grains readily (CNO, S and Zn), and sharp (shell-like) absorption lines. The two WLM stars do bear some resemblance to post-AGB stars, other than significantly higher N and O abundances relative to the iron-group; see Section 4. However, it is very unlikely that two foreground, Galactic post-AGB stars will be found in the WLM field, with the same radial velocity as the HI in WLM, and with the same abundances as each other.

### 3.3. Supergiants in WLM

The two supergiants presented here are amongst the brightest single stars in the galaxy (membership discussed in Section 3.2). That they are low luminosity Ib supergiants begs the question “Where are the Ia supergiants?”. This same question was asked by Sandage & Carlson (1985) when they could not find Cepheid variables in WLM with periods of more than 10 days<sup>6</sup>. The most likely explanation for the missing high mass stars is that WLM has had an interrupted star formation history during the past 10 Myr (also see the discussion by Skillman et al. 1989a). The star formation history for WLM has been examined by Dolphin (2000) from HST WFPC2 imaging (discussed in Section 6.2), but the youngest age bin is 0 to 200 Myr, much larger than the supergiant lifetimes.

Another possibility is that these stars *are* the higher mass Ia supergiants masquerading as Ib’s due to a high surface helium abundance. Helium has the effect of increasing the electron density through an increase in the mean molecular weight in the atmosphere, as noticed by Kudritzki (1973). An increase in density primarily mimics an increase in the surface gravity, e.g., exhibited in the Balmer line profiles through intensified Stark broadening. Increasing helium from 9% to 40% in the model atmosphere of WLM-15 mimics a decrease in gravity of only 0.3 dex, i.e., the Balmer lines and Mg I/Mg II ionization equilibrium are fully recovered. This occurs at the same  $T_{\text{eff}}$  (which does imply a shift in the Mg I/Mg II balance), but surprisingly results in nearly the same LTE abundances overall; see Table 5. The lower gravity would also suggests a higher mass than we have adopted in Section 3.2;

---

<sup>6</sup>Note that the missing Cepheid variables would have masses  $\geq 7 M_{\odot}$ , whereas the two supergiants in this paper have  $M \sim 12 M_{\odot}$

from the LeJeune & Schaerer (2001) evolution tracks, the stellar mass of a Ia supergiant with  $\log g = 1.3$  is  $\sim 20 M_{\odot}$ . Such a high mass and low gravity would result in an inconsistent distance modulus for WLM-15 ( $D_{WLM-15} \sim 1500$  kpc). We do note however that some small increase in helium is likely in WLM-15 since there is an enrichment in the surface nitrogen abundance, see Section 4. The distance modulus for WLM-31 would be even larger since the A-supergiant blended in WLM-31 is fainter (see the discussion in Section 3.2). Thus, we cannot rule out a helium effect, but also we cannot quantify it at present; fortunately, we notice it would not play any significant role in the resulting *abundances*.

#### 4. Abundances

Elemental abundances have been calculated from an absorption line equivalent widths analysis, as well as spectrum synthesis for WLM-15. All calculations have been done using a modified version of LINFOR<sup>7</sup>. The line list and atomic data were initially adopted from previous A-supergiant analyses (Venn 1995a,b, 1999; Venn et al. 2001), and updated when appropriate, as listed in Table 3. An attempt has been made to adopt laboratory measurements (e.g., O’Brien et al. 1991 for Fe I) and Opacity Project data (e.g., Hibbert et al. 1991 for O I). Critically examined data were selected next (e.g., NIST data from Fuhr, Martin, & Wiese 1988 for Fe II), followed by the semiempirical values calculated by Kurucz (1988).

Average elemental abundances<sup>8</sup> for each star are listed in Table 4 and shown in Fig. 5. Two error estimates are noted per element: the first is the line-to-line scatter ( $\sigma$ ) and the second is an *estimated* systematic uncertainty in the atmospheric parameters ( $T_{\text{eff}}$ , gravity, and  $\xi$ ). Abundance uncertainties due to the model atmospheres are shown in Table 5. It is clear from this table that O I, Mg II, Cr II, and Fe II are amongst the most reliable abundance determinations. The systematic error is probably an overestimate since we have simply added the possible uncertainties in quadrature, not accounting for the fact that some  $T_{\text{eff}}$ -gravity combinations are excluded by the data. Scaling the metallicity in the model atmosphere’s opacity distribution function to 1/3 solar had a negligible effect on these abundances ( $\leq 0.04$  dex). For comparison, solar abundances in Table 4 are from Grevesse & Sauval (1998), with

---

<sup>7</sup>LINFOR was originally developed by H. Holweger, W. Steffen, and W. Steenbock at Kiel University. Since then, it has been upgraded and maintained by M. Lemke, with additional modifications by N. Przybilla. It can be obtained at the following web address: <http://www.sternwarte.uni-erlangen.de/pub/MICHAEL/ATMOS-LINFOR-NLTE.TGZ>.

<sup>8</sup>Note that abundances are determined from spectral lines of a particular ionization state of an element, but the result is the *total abundance* of that element since ionization fractions are implicitly calculated in a model atmospheres analysis.

the exceptions of N and O = 7.80 and 8.66, respectively, from Asplund (2003).

For WLM-15, spectrum syntheses were performed over several wavelength regions, including all of the Mg line regions, as well as the region around O I  $\lambda$ 6158 and N I  $\lambda$ 7440 (see Figs 6 and 7). Macroturbulence equal to  $9 \text{ km s}^{-1}$  was adopted based on the instrumental resolution and set-up of the UVES spectrograph (R=45,000 with a  $1.0''$  slit, then 2x2 binning yields an optimal resolution of  $\sim 9.4 \text{ km s}^{-1}$ ). Remaining broadening is attributed to  $v \sin i$  ( $\sim 7 \pm 1 \text{ km s}^{-1}$ ). Spectrum syntheses were not performed for WLM-31 because of the continuum offset due to the RGB blend (see Section 3.1), however comparison of WLM-31 and WLM-15 shows that the spectra have nearly identical broadening.

*Iron-group:* The iron group abundances are in remarkably good agreement from lines of Fe I, Fe II, CrI, and CrII, with the mean abundance  $\langle [(\text{Fe,Cr})/\text{H}] \rangle = -0.36 \pm 0.17$  ( $\pm 0.30$ ) from both stars. The Fe II and Cr II abundances (from several absorption lines each) are the most reliable, and show only small sensitivities to the atmospheric parameter uncertainties. Furthermore, NLTE corrections are predicted to be small for these dominant ionization states.

Sc and Ti can be considered as either iron-group or  $\alpha$  elements. The Ti abundances are determined from several lines and are in excellent agreement with iron,  $[\text{Ti}/\text{Fe}] = +0.07 \pm 0.21$  ( $\pm 0.27$ ). The Sc II abundances are in fair agreement with the iron-group, although from far fewer lines and showing a larger temperature sensitivity; furthermore, hyperfine structure (the presence of a nuclear magnetic moment for lines of odd elements of the iron-group) has been neglected. This should produce a negligible error in this weak line analysis, and the differential Sc II results (below) should be more reliable.

*The  $\alpha$ -elements (Mg, O, and Si):* The mean abundance of magnesium from several lines of two ionic species in both WLM stars is  $[\text{Mg}/\text{H}] = -0.62 \pm 0.09$  ( $\pm 0.26$ ), which is slightly lower than the iron-group result. Mg II is particularly reliable being rather insensitive to the typical uncertainties in temperature and gravity, and is found to suffer from negligible NLTE corrections (see Section 3). Intriguingly, this contrasts with the oxygen abundance determined from spectrum synthesis of the  $\lambda$ 6158 feature (see Fig. 6) in WLM-15. In LTE, the best fit is with  $12+\log(\text{O}/\text{H})=8.60$ , and we apply a NLTE correction of  $-0.15$  (Przybilla et al. 2000, based on the atmospheric parameters). Thus, the NLTE abundance listed in Table 4 is  $[\text{O}/\text{H}] = -0.21 \pm 0.10$  ( $\pm 0.05$ ) (note that 0.10 dex is adopted as the line-to-line scatter based on the S/N of the spectrum and continuum placement in the spectrum synthesis). An equivalent width analysis of the 6158 Å line alone results in the same abundance. This result is 2.5 times larger than the magnesium abundance relative to solar, and 5 times larger than the nebular oxygen abundance! The oxygen uncertainties in Table 5 are determined from the  $W_\lambda$  analysis of the 6158 Å line abundance. Oxygen is not determined in WLM-31; at

6200 Å the WLM A-supergiant is expected to contribute only  $\sim 13\%$  to the continuum (from the Kurucz fluxes, discussed earlier) which is insufficient to measure the weak O I lines, especially compared to stronger features in that region of the red giant spectrum.

Si appears to be the most underabundant element in these stars with the mean  $[\text{Si}/\text{H}] = -0.81 \pm 0.15$  ( $\pm 0.28$ ). However, Si abundances have been found to vary by over a factor of 10 from star to star amongst the A-supergiants in the SMC and the Galaxy (Venn 1995b, 1999), including large underabundances not supported by the other element ratios. It is not clear if this is due to neglected NLTE corrections, although it is possible since Si III would be the dominant ionization state at these temperatures. Thus, the underabundance of Si in WLM may not be significant. The Si abundances are discussed further below in Section 5.

*Nitrogen:* Nitrogen can be determined in WLM-15 from N I lines near  $\lambda 7440$  (see Fig. 7). In LTE, the best fit is for  $12 + \log(\text{N}/\text{H}) = 8.0$ , but a NLTE correction ( $-0.50$ ) is determined here using the departure coefficients calculated for the SMC stars AV392 and AV463 by Venn (1999). These departure coefficients are *not* strongly affected by the new collisional excitation cross-sections (calculated by Frost et al. 1998, and discussed for A-type supergiants by Przybilla 2001b) because of the cool temperature of the atmosphere. Additionally, while the NLTE corrections are quite large, the differential nitrogen abundances with respect to the SMC stars (particularly AV463) should be more certain (Section 5). The NLTE abundance is  $[\text{N}/\text{H}] = -0.30 \pm 0.10$  ( $\pm 0.04$ ) (note that 0.10 dex is adopted as the line-to-line scatter based on the S/N of the spectrum and continuum placement in the spectrum synthesis). An equivalent width analysis of the 7440 and 7462 Å lines results in the same abundance as the spectrum synthesis, thus the nitrogen uncertainties in Table 5 are determined from these two lines. The nitrogen underabundance is about 1/3 solar, which is much higher than the mean nebular nitrogen result from HM95 below 1/10 solar. However, HM95 note the N/O abundances are quite uncertain, with an upper limit of  $12 + \log(\text{N}/\text{H}) \leq 7.30$  that is close to our stellar value.

*s-process elements:* One line each of Zr, Ba, and Sr appear to be unblended in the spectra of both WLM stars. The Zr II  $\lambda 4149$  and Ba II  $\lambda 4934$  results in both stars suggest  $[\text{s}/\text{Fe}]$  ratios near solar; the mean value  $\langle [\text{Zr}, \text{Ba}/\text{Fe}] \rangle = +0.08 \pm 0.20$  ( $\pm 0.35$ ). This is not surprising if iron is predominantly from SNe Ia and the s-process abundances from AGB stars, with a similar timescale for enrichment. The Sr II  $\lambda 4077$  line abundance is significantly lower,  $\langle [\text{Sr}/\text{Fe}] \rangle = -1.1$ , as has been seen in other A-supergiant analyses. For example, the mean ratio of  $[\text{Sr}/\text{Fe}]$  in 10 SMC A-supergiants was also  $-1.0$  dex (Venn 1999). Belyakova et al. (1999) suggest that Sr II abundances in A-stars suffer from metallicity dependent NLTE effects. This would also explain why the mean  $[\text{Sr}/\text{Fe}]$  ratio in Galactic A-supergiants is only  $-0.4$  dex (Venn 1995b).

## 5. Differential Abundances

The absolute abundances determined above are compared to the analyses of similar stars in other galaxies in this Section, because systematic uncertainties in atomic data and model atmosphere assumptions may be reduced through a differential comparison. In particular, we will examine the patterns in abundances and ratios between the two stars in WLM and previously studied A-supergiants in the Galaxy, SMC, and NGC6822 (Venn 1995a,b, 1999, Venn et al. 2001). Sample spectral regions for the WLM stars and the comparison stars, SMC-AV392, SMC-AV463, NGC6822-cc, and Galactic-HD34578, are shown in Figs. 6 and 8. The spectra for NGC6822-cc was taken at the Keck telescope with HIRES by J.K. McCarthy (analysed in Venn et al. 2001), those for the SMC stars were taken at the ESO 3.6-meter telescope with CASPEC (Venn 1999), and those for the Galactic star HD 34578 were taken with the 2.1-meter telescope at the McDonald Observatory with the coudé spectrograph (Venn 1995a,b). All of the spectra have high resolution, with  $40,000 \leq R \leq 60,000$  per pixel. Differential abundances are listed in Tables 6 and 7 and shown in Fig. 9. When there are relatively few lines in the analysis (e.g., O I, Mg I, Mg II, Si II, and the s-process elements), then abundance results have been compared line by line and averaged (instead of comparing the mean abundances resulting from slightly different line sets).

*Comparison with NGC6822-cc:* The similarities between NGC6822-cc and the two WLM stars in Figs. 6 and 8 are striking; the metal lines are extremely sharp<sup>9</sup> with nearly identical line strengths. These three stars have nearly the same temperature and metallicity, but NGC6822-cc’s higher luminosity is apparent from the sharper Balmer line in Fig. 8. Unlike the absolute abundances, these differential abundances show that the O/Fe and Si/Fe ratios are the same between these two stars. Presumably, this is because similar uncertainties in the atmospheric analyses cancel. The differential Mg/Fe ratio is consistent with the absolute abundance [Mg/Fe] ratio though, and supports that [Mg/Fe] is less than the solar ratio in WLM-15. (We also note that the differential Sc/Fe appears to be severely underabundant, however NGC6822-cc has an unusually large Sc abundance which may not be reliable).

*Comparison with SMC-AV463, SMC-AV392, and HD 34578:* The differences between the WLM spectra and those for the Galactic and SMC comparison stars are also striking in Figs. 6 and 8 (besides the S/N). It is obvious that the SMC stars are more metal-poor

---

<sup>9</sup>It is not clear why the absorption lines are so sharp in the two WLM stars and NGC6822-cc, but not in the Galactic nor SMC comparisons (which have average rotation rates of  $\sim 20 \text{ km s}^{-1}$ ). The sharpness implies a very low intrinsic rotation rate since it is unlikely that three of the brightest stars in WLM and NGC6822 also happen to be pole-on rotators. Since the SMC is more metal-poor than these stars, these low rotation rates do not appear to be related to metallicity.

than the Galactic star, but due to differences in the broadening parameters (and, to a lesser degree, slight differences in the atmospheric parameters), it is not clear where the WLM stars fall in metallicity without the detailed model atmospheres analysis. Comparing WLM-15 to two SMC A-supergiants (AV392 which is slightly hotter, and AV463 which is slightly cooler), WLM-15 is clearly more metal-rich in iron-group elements by  $\sim 0.2$  dex. However, the O/Fe ratio is the same between these three stars (and NGC6822-cc as well). The differential Mg/Fe ratio is suppressed relative to AV463, and it is marginally lower than in AV392.

Other differential abundances relative to the SMC stars are also interesting. The differential Si/Fe ratio supports the absolute abundance result that Si is suppressed, in contrast to the differential result relative to NGC6822-cc. Since Si abundances vary significantly from star-to-star in the SMC and Galaxy, this may reflect the true uncertainty in the Si abundances (i.e., larger than expected from simple errors in the atmospheric parameters, possibly due to neglected NLTE effects). It also shows the importance of choosing a comparison star. An even larger range in differential abundances is seen for the Sr/Fe ratios, which is due to the large range in Sr in the SMC stars themselves. While this might be related to neglected (and metallicity-dependent) NLTE effects, we note that NLTE corrections are usually similar between similar stars. Perhaps there is a true range in the strontium abundances in the SMC stars, which could be related to inhomogeneous mixing of Sr from AGB stars in the SMC’s interstellar medium. Perhaps this is also true for silicon.

The differential N/Fe ratio is in good agreement between WLM-15 and SMC-AV463. In the SMC, a wide range of nitrogen abundances were found and interpreted as evidence for rotational mixing during the main-sequence lifetime (which would vary from star to star depending on their rotational velocity and mass, Venn 1999a). The simple interpretation then would be that WLM-15 has a mass and had a main-sequence rotation rate that are similar to AV463.

Finally, a comparison of WLM-15 to the Galactic A-supergiant, HD 34578, a slightly less luminous supergiant, shows no significant differences from the absolute abundance ratios (relative to solar).

*Summary:* The differential abundances suggest that the range in the abundance ratios are within the normal range seen in other A-type supergiants in other galaxies. Thus, small differences ( $\leq 0.2$  dex) between the abundance ratios are most likely related to model atmosphere analysis uncertainties. However, the differential comparisons support that the Mg/Fe ratios are less than solar in WLM, and that the O/Fe ratio in WLM-15 may not be significantly above solar as suggested by the absolute abundances. Thus, the O/Mg ratio does appear higher in WLM-15 than the comparison stars. Oxygen in the stars and nebulae in the SMC and NGC6822 were in excellent agreement (discussed by Venn 1999, Venn

et al. 2001). Thus, the discrepancy in oxygen between the stellar and nebular abundances in WLM is significant. Finally, there is a large range seen in the differential abundances of Si/Fe and Sr/Fe (it is not clear if this reflects a true scatter in the star-to-star abundances within a galaxy), while the *lack* of a large difference in the N/Fe ratios between WLM-15 and SMC-AV463 suggest similar main-sequence rotational mixing histories.

## 6. Discussion

Part of the motivation for determining the stellar abundances in WLM has been to look for variations in the [O/Fe] ratio between different dwarf irregular galaxies. Differences in [O/Fe] imply significantly different star formation histories (Gilmore & Wyse 1991) or differences in infall or outflow (assuming constant IMFs and stellar yields). Therefore, variations in the O/Fe ratios between galaxies seem likely.

### 6.1. The Metallicity and Oxygen Abundances in WLM

The metallicity determined here for the two young ( $\leq 10$  Myr) supergiants in WLM is  $[\text{Fe}/\text{H}] = -0.38 \pm 0.20$  ( $\pm 0.29$ ). Reliable magnesium abundances are determined from several lines of two ionization states in both stars resulting in  $[\text{Mg}/\text{H}] = -0.62 \pm 0.09$  ( $\pm 0.26$ ). These results suggest that the stars are significantly more metal-rich than the reported nebular oxygen abundances,  $12 + \log(\text{O}/\text{H}) = 7.77 \pm 0.17$  from HM95, or  $[\text{O}/\text{H}] = -0.89$ . Oxygen is determined in only one WLM supergiant, WLM-15, from spectrum synthesis of the O I 6158 feature, resulting in  $[\text{O}/\text{H}] = -0.21 \pm 0.10$  ( $\pm 0.05$ ) (adopting the fitting accuracy for the line scatter uncertainty as mentioned previously in Section 4), which is even more discrepant with the nebular oxygen abundance. Why are the stellar and nebular abundances different by 0.68 dex ( $>3\sigma$ )? This seems impossible astrophysically since these stars are young and presumably formed from the present-day interstellar medium sampled by the H II regions. Possible mechanisms to create an offset are discussed below.

#### 6.1.1. Could the nebular measurements of O/H be too low?

Two of the 21 H II regions in WLM (WLM-HM7 and WLM-HM9) are bright enough that HM95 were able to detect the [O III]  $\lambda 4363$ , but only WLM-HM7 has a firm measurement, where  $I(\lambda 4363)/I(\text{H}\beta) = 0.09 \pm 0.01$ , and thus direct measure of the temperature in the  $\text{O}^{++}$  regions. The line ratio in WLM-HM9 is  $I(\lambda 4363)/I(\text{H}\beta) = 0.05 \pm 0.06$ . The only other

measurements of abundances in WLM are for two H II regions by Skillman et al. (1989a); one of these is in common with HM95 (WLM#1 = WLM-HM9), and again the [O III]  $\lambda 4363$  line was detected with a large uncertainty (line ratio relative to  $H\beta$  was  $0.08 \pm 0.06$ ), and similar for a second H II region (WLM#2 = WLM-HM2, with an [O III] line ratio of  $0.15 \pm 0.12$ ). Although all four oxygen abundance estimates are in agreement, considering the significant uncertainties in the nebular temperatures, it remains plausible that the nebular oxygen abundances in WLM could be higher than the existing estimates by as much as 0.2 dex. Additionally, low surface brightness H II regions may have relatively large temperature fluctuations (e.g., Peimbert 1993, Esteban 2002) which would lead to underestimates of the true nebular oxygen abundances. New observations of the H II regions in WLM are needed to examine this further.

The low value of O/H is consistent with the non-detection of CO and the metallicity-luminosity relationship for dwarf irregular galaxies. Taylor & Klein (2001) found no CO emission in WLM, which is consistent with an oxygen abundance of  $12+\log(O/H) \leq 7.9$ . Other, more distant, galaxies with oxygen abundances above 8.1 have been detected in CO. The metallicity-luminosity relationship for dwarf irregulars is shown in Fig. 10 as the oxygen abundance versus blue magnitudes  $M_B$  from Richer & McCall (1995). The stellar oxygen abundance for WLM-15 lies well above this relationship. The mean [Mg/H] underabundance is in better agreement though (plotting  $12+\log(O/H)_{\odot} + [Mg/H]$ ); in fact it is in excellent agreement with NGC6822, which also lies above the relation. Thus, if the stellar [Mg/H] ratio is a better estimate of the  $\alpha$  element abundances in WLM, then its position is consistent with the scatter in the metallicity-luminosity relationship.

### 6.1.2. *Could the stellar measurements of O/H be too high?*

To reduce the stellar oxygen abundance in WLM-15 to the nebular value requires reducing the temperature by  $\sim 800$  K with no change in gravity, or increasing  $\log g$  by  $\sim 1.0$  with no change in temperature. These would be very large changes indeed;  $4\sigma$  in the temperature of WLM-15, or  $10\sigma$  in its gravity. These changes would not reproduce the Balmer lines nor Mg I/Mg II (and Fe I/Fe II) ionization equilibrium, thus it is not possible to reproduce the nebular oxygen abundance in the stellar spectrum of WLM-15 (also see Fig. 6). To further investigate the stellar oxygen abundances in the WLM dwarf galaxy will require high resolution observations of additional stars. In particular, analysis of B-type supergiants will permit a more reliable determination of the stellar oxygen abundance in WLM from the numerous O II lines.

### 6.1.3. Possible mechanisms to create an offset.

If future observations support the  $\Delta(\text{O}/\text{H}) = 0.68$  dex difference between the stellar and nebular oxygen abundances, then we consider the following possible scenarios that could produce this offset.

1. *Has the nebular oxygen been diluted by infall of metal-poor H I gas?* Taylor et al. (1995) have shown that H II galaxies can have companion H I clouds. The HIPASS survey (Putman et al. 2002) shows there are high velocity clouds in the direction of WLM, some with similar radial velocities that may suggest an association with WLM. None are particularly close to WLM and all have low H I masses (e.g., HVC 066.1-69.6-172 is the most significant cloud at 1.25 kpc distance with 43% of the H I flux of WLM), but could an H I cloud have recently merged with WLM? Gas infall could dilute the interstellar medium in WLM. If both the stellar and nebular abundances are accurate, this would have had to happen in a very short timescale,  $\leq 10$  Myr ( $\sim$  age of the massive supergiants). Also, the mass of the H I would have had to be high ( $\geq 10^6 M_{\odot}$ ) to dilute the ISM by at least 50%. These two requirements seem unlikely. Unfortunately, no detailed H I mapping is currently available for WLM to search for kinematic structures that might be associated with a recent merger.

2. *Large Spatial Variations?* The two stars examined here and the two H II regions examined by HM95 (and an additional H II region by Skillman et al. 1989) are located in the south and central regions of the bar of WLM, see Fig. 1. Both stars are on the east side, whereas the nebulae are on the west side. Could the difference in the abundances be an indication of spatial variations in the oxygen abundance in WLM? The higher oxygen abundances in the stars on the east side may have formed from a small gas cloud recently polluted in oxygen over a small volume (e.g., by a local SN II event which may have also triggered the star formation). Evidence for immediate enrichment in oxygen in star forming regions are currently inconclusive. Kobulnicky & Skillman (1996, 1997) found no evidence for localized oxygen enrichments from nebular analyses in NGC 1569 nor NGC 4214 (also, Martin et al. 2002 report higher oxygen abundances in the hot X-ray gas around NGC 1569 suggesting the newly synthesized material is injected into the ISM in the hot phase with an uncertain cooling and mixing timescale). However, Cunha & Lambert (1994) find a marginally higher oxygen abundance in B-stars in the youngest (Id) subcluster in the Orion star forming complex. The similarity in the oxygen abundances between the two H II regions in WLM reported by HM95 (and a third by Skillman et al. 1989) would suggest that there are no large spatial variations in WLM. The similarities in the magnesium and iron-group abundances in the two A-supergiants in WLM also argues against spatial variations. Spectral analyses of additional low surface brightness H II regions and young stars throughout WLM are needed to address this problem further.

3. *Changes in the Gas-to-Dust Ratios?* Most analyses of gas-phase abundances along sight lines to stars in the SMC (Sk 108, Sk 78) have shown broadly similar relative abundance patterns to those found for the Galactic ISM (Welty et al. 1997, Mallouris et al. 2001). That is, the light elements Mg and Si show mild, monotonic depletions with the iron-group elements, and these variations are attributed to different environments in the Galaxy (cold dense cloud, warm diffuse cloud, and halo cloud patterns). However, recent analyses towards Sk 155 in the wing of the SMC shows a significantly different gas-phase abundance pattern (Welty et al. 2001). In particular, Mg and Si appear to be relatively undepleted onto dust grains, whereas the iron-group show moderate to severe depletions. This has not been seen in any Galactic sight line. Welty et al. suggest that models of the SMC dust, which currently rely heavily on silicates, could be modified to have a dominance of oxides and/or metallic grains as an alternative. Sofia et al. (1994) also concluded that oxides and/or metallic grains could comprise a substantial fraction of the Galactic dust. If this is extended to WLM, perhaps the low nebular oxygen abundance is due to substantial oxygen being locked in dust grains. However, the difference in between the nebular oxygen and stellar oxygen found here would suggest that >50% of the gas-phase oxygen has been depleted into dust, a much larger fraction than seen anywhere else in the Galaxy or SMC.

## 6.2. Chemical Evolution of WLM

The iron-group abundances in the two WLM stars suggest that this galaxy is more chemically evolved than modelled by Dolphin (2000) who used HST WFPC2 imaging of a small portion of WLM to reconstruct its star formation history and chemical evolution from its color-magnitude diagram. Dolphin’s analysis suggests that half of WLM’s total star formation (by mass) formed before 9 Gyr ago, then the star formation activity slowly declined until a recent increase, starting between 1 and 2.5 Gyr ago, concentrated in the bar. He predicts a current metallicity of only  $[\text{Fe}/\text{H}] = -1.08 \pm 0.18$ . Dolphin also notes that this predicted metallicity is in good agreement with the nebular oxygen value by HM95, thereby suggesting an  $[\text{O}/\text{Fe}]$  ratio that is consistent with the solar ratio.

It is not clear that our stellar abundances are consistent with a solar  $\alpha/\text{Fe}$  ratio. The absolute abundances suggest that  $[\text{Mg}/\text{Fe}]$  is less than the solar ratio in both stars, whereas  $[\text{O}/\text{Fe}]$  may be slightly enhanced in WLM-15. The differential abundances agree that Mg/Fe is suppressed, but that O/Fe is consistent with the stellar ratios in NGC6822 and the SMC (where the mean stellar oxygen abundances *are* in agreement with the nebular results). Therefore, if we neglect the high stellar oxygen abundance in WLM-15, and focus on the more reliable Mg abundance as the  $\alpha$  abundance indicator, then we find that WLM is the

first dwarf irregular galaxy that appears to have an  $\alpha/\text{Fe}$  ratio that is less than solar in the Local Group.

A less than solar  $\alpha/\text{Fe}$  ratio implies a rapid decline or hiatus in the star formation; based on Dolphin’s model for WLM, this would have occurred between 1 and 9 Gyr ago. During this time, significant SNe Ia enrichment would occur without SNe II enrichment, lowering the  $\alpha/\text{Fe}$  ratio. This also implies that little/no mixing of the SNe II products from the current star formation activity has occurred, but the timescale for mixing of SNe II products is not well known and possibly longer than  $\sim 1$  Gyr (e.g., Kobulnicky & Skillman 1996, 1997; Martin et al. 2002).

Finally, the overall similarities between NGC6822-cc and WLM-15 (supported by WLM-31) suggest a very similar chemical evolution history (or at least chemical evolution end point) for these two galaxies. The star formation history in NGC6822 has been examined from its ground-based (2.5-meter Isaac Newton Telescope, Canary Islands) color-magnitude diagram by Gallart et al. (1996a,b). Similar to WLM, Gallart et al. find that NGC6822 formed most of its stars by intermediate ages, reaching half of its current metallicity  $\sim 6$  Gyr ago. They find a final metallicity of 1/5 solar, which is slightly lower than the stellar and nebular abundance results in NGC6822 of 1/3 solar. There was little star formation activity in NGC6822 from  $\sim 6$  Gyr ago until recently,  $\sim 1$  Gyr ago, with particularly strong and localized activity in the past 100-200 Myr (leading to spatial abundance variations?). Dolphin’s analysis also shows significant differences in the very recent ( $\leq 1$  Gyr) star formation activity between the different WFPC2 WF fields, thus different parts of the WLM galaxy. The difference in the Mg/Fe ratios between the stars in these two galaxies (see Section 5) may be related to differences in the length of time of the star formation hiatus in these galaxies and/or age when SN Ia began to contribute Fe. The difference in Mg/Fe could also be related to any number of other chemical evolution parameters though (e.g.,  $\alpha$ -element losses in a galactic wind). A study of the star formation history in WLM from a color-magnitude diagram that covers the entire galaxy would make it possible to study the progression of the recent activity across the galaxy more carefully.

## 7. Conclusions

We have presented VLT UVES spectroscopy of bright A-type supergiants in the dwarf irregular galaxy WLM. Model atmospheres analyses of the two supergiants, WLM-15 and WLM-31, yield their chemical composition (after WLM-31’s spectrum was recovered from a blend with a foreground red giant). The abundances are in excellent agreement between the two stars, yielding a metallicity of  $[\text{Fe}/\text{H}] = -0.38 \pm 0.20$  ( $\pm 0.29$ ). This metallicity is

supported (within 0.1 dex) by the abundance results for Na, Ti, and Cr. The magnesium abundances are slightly lower,  $[\text{Mg}/\text{Fe}] = -0.24 \pm 0.16$  ( $\pm 0.28$ ). The ratio of the other  $[\alpha/\text{Fe}]$  elements varies from +0.2 (O) to  $-0.4$  dex (Si), although this pattern changes when differential abundances (relative to similar stars in NGC6822, the SMC, and the Galaxy) are examined. The lower  $[\text{Mg}/\text{Fe}]$  persists, but the differential  $[\text{O}/\text{Fe}]$  ratio, and often the  $[\text{Si}/\text{Fe}]$  ratio, is consistent with solar. If we use the more reliable Mg abundances as the  $\alpha$  element indicator (more absorption lines analysed, from two ionization states, with NLTE corrections included, and with agreement from both stars), then the  $[\alpha(\text{Mg})/\text{Fe}]$  ratio in WLM suggests this ratio is less than the solar value. This is the first time this has been seen in a Local Group galaxy, and may be related to a hiatus at intermediate ages in its star formation history. We also notice that the similarities between WLM-15 and NGC6822-cc (Venn et al. 2001) are striking, suggesting that WLM and NGC6822 may have had very similar star formation histories (Dolphin 2000, Gallart et al. 1996a,b). The only exception is that the stars in WLM have a lower Mg/Fe ratio than those in NGC6822, which may be related to differences in the length of the star formation hiatus in these galaxies.

The metallicity determined from the two WLM stars in this paper is *not* in agreement with the nebular oxygen abundance from H II regions in WLM (Hodge & Miller 1995, Skillman et al. 1989a). The nebular oxygen abundance is much lower, reported as  $12+\log(\text{O}/\text{H}) = 7.77 \pm 0.17$ , or  $[\text{O}/\text{H}] = -0.89$ . There is no simple explanation for this since these are young stars that should have formed from the present-day interstellar medium sampled by the H II regions. We have considered whether the interstellar medium in WLM could have been diluted by a companion H I cloud (Taylor et al. 1995), but it seems unlikely since a high mass ( $10^6 M_{\odot}$ ) cloud would need to have merged and rapidly mixed within the past 10 Myr. We have also considered whether gas-phase oxygen could be depleted onto oxide dust grains (Welty et al. 2001, Sofia et al. 1994), but over half of the interstellar oxygen would have to be locked in dust grains which is much more than seen in the Galaxy or SMC. Temperature fluctuations (Peimbert 1993, Esteban et al. 2002) would move the nebular abundances into better agreement with the stellar results, particularly if the stars have less than solar  $\alpha/\text{Fe}$  ratios. The new stellar metallicity presented here pushes WLM above the metallicity-luminosity relationship (Richer & McCall 1995) observed for traditional dwarf galaxies. New observations of nebular abundances, stellar abundances, and a galaxy wide color-magnitude diagram are all modern methods that can be used to better understand the evolution of WLM.

We thank the Paranal Observatory staff for excellent support during our visitor run. Special thanks to Thomas Szeifert for showing us his FORS2 spectra of WLM supergiants at the telescope, thanks to Max Pettini for help estimating upper-limits to the nebular column

densities towards our target stars, and also thanks to Norbert Przybilla for many stimulating discussions on detailed analyses of A-type supergiants. We would also like to acknowledge several helpful questions and suggestions by the referee (anonymous). KAV would like to thank the NSF for support through a CAREER award, AST-9984073; most of this work was done during a long-term visit at the Institute of Astronomy, University of Cambridge, UK. ET gratefully acknowledges support from a fellowship of the Royal Netherlands Academy of Arts and Sciences, and PATT travel support from University of Oxford. SJS thanks PPARC for Advanced Fellowship funding.

## REFERENCES

- Allende-Prieto C., Lambert D.L., Asplund M., 2001, *ApJ*, 556, 63
- Asplund, M., in *CNO in the Universe*, ed. C. Charbonnel, D. Schaerer, G. Meynet (San Francisco:ASP), in press
- Becker S.R., 1998, in *ASP Conf. Ser. 131, Boulder-Munich Workshop II: Properties of Hot, Luminous Stars*, ed. I.D. Howarth (San Francisco: ASP), 135
- Belyakova E.V., Mashonkina L.I., Sakhbullin N.A., 1999, *Astronomy Reports*, 43, 819
- Bonifacio P., Hill V., Molaro P., Pasquini L., Di Marcantonio P., Santin P., 2000, *A&A*, 359, 663
- Boyarchuk A.A., Lyubimkov L.S., Sakhbullin N.A., 1985, *Astrophysics*, 21, 203
- Chiappini C., Matteucci F., Gratton R., 1997, *ApJ*, 477, 765
- Clayton, D.D. 1988, *MNRAS*, 234, 1
- Cunha K., Lambert D.L., 1994, *ApJ*, 426, 170
- Dekker, H., D’Odorico, S., Kaufer, A., Delabre, B., & Kotzlowski, H., 2000, in ”Optical and IR Telescope Instrumentation and Detectors”, Masnori Iye and Alan F. Moorwood (Eds.), *Proc. SPIE Vol. 4008*, p. 534
- Dolphin A.E., 2000, *ApJ*, 531, 804
- Edvardsson, B., Andersen, J., Gustafsson, B., Lambert, D.L., Nissen, P.E., & Tomkin, J. 1993, *A&A*, 275, 101
- Esteban, C., Peimbert M., Torres-Peimbert S., Rodríguez M., 2002, *ApJ*, 581, 241

- Ferraro F.R., Fusi Pecci F., Tosi M., Buonanno R., 1989, MNRAS, 241, 433
- Frost R.M., Awakowicz P., Summers H.P., Badnell N.R., 1998, Journal of Applied Physics, 84, 2989
- Fuhr J.R., Martin, G.A., Wiese W.L., 1988, J. Phys. Chem. Ref. Data, 17, Suppl. 4
- Fuhr J.R., Martin, G.A., Wiese W.L., Younger S.M., 1981, J. Phys. Chem. Ref. Data, 10, 305
- Fuhr J.R., Wiese W.L., 1998, in CRC Handbook of Chemistry and Physics, ed. D.R. Lide (79th ed.; Boca Raton: CRC), 1232
- Gallart, C., Aparicio A., Bertelli G., Chiosi C., 1996a, AJ, 112, 1950
- Gallart, C., Aparicio A., Bertelli G., Chiosi C., 1996b, AJ, 112, 2596
- Gigas D., 1988, A&A, 192, 264
- Gigas D., 1986, A&A, 165, 170
- Gilmore, G., Wyse R.F.G., 1991, ApJ, 367, L55
- Grebel E.K., 1997, Rev. Mod. Astron., 10, 29
- Grevesse N., Sauval A.J., 1998, Space Sci. Rev., 85, 161
- Hibbert A., Biéumont E., Godefroid M., Vaeck N., 1991, J. Phys B, 24, 3943
- Hill V., et al., 2003, in prep.
- Hill V., 1999, A&A, 345, 430
- Hill V., 1997, A&A, 324, 435
- Hill V., Andrievsky, S., Spite, M., 1995, A&A, 293, 347
- Hobbs, L.M., 1974, ApJ, 191, 381
- Hodge, P., Miller B.W., 1995, ApJ, 451, 176
- Hodge, P., Dolphin A.E., Smith T.R., Mateo M., 1999, ApJ, 521, 577
- Hodge, P., 1989, ARA&A, 27, 139
- Huchtmeier W.K., Richter O.G., 1986, A&ASuppl., 63, 323

- Hurley-Keller D., Mateo M. & Nemec J. 1998, *AJ*, 115, 1840
- Hunter D.A., Hunsberger S.D., Roye E.W., 2000, *ApJ*, 542, 137
- Kobulnicky H.A., Skillman E.D., 1996, *ApJ*, 471, 211
- Kobulnicky H.A., Skillman E.D., 1997, *ApJ*, 489, 636
- Kudritzki, R.P., 1973, *A&A*, 28, 103
- Kurucz, R.L., 1979, *ApJS*, 40, 1
- Kurucz, R.L., 1988, *Trans. IAU*, Vol. 20B, ed. M. McNally (Dordrecht: Kluwer), 168
- Kurucz, R.L., 1993, CD-rom No.13, Cambridge, Mass.: Smithsonian Astrophysical Observatory
- Lejeune T., Schaerer D., 2001, *A&A*, 366, 538
- Lee M.G., Freedman, W.L., Madore B.F., 1993, *ApJ*, 417, 553
- Luck R.E., Moffett T.J., Barnes T.G., Gieren W.P., 1998, *AJ*, 115, 605
- Mallouris C., et al., 2001, *ApJ*, 558, 133
- Martin, C.M., Kobulnicky H., Heckman T., 2002, *ApJ*, 574, 663
- Martin, G.A., Fuhr, J.R., Wiese W.L., 1988, *J. Phys. Chem. Ref. Data*, 17, Suppl. 3
- Mateo, M. 1998, *ARA&A*, 36, 435
- Matteucci, F., Tosi M., 1985, *MNRAS*, 217, 391
- Matteucci, F., Greggio L., 1986, *A&A*, 154, 279
- Matteucci, F., Raiteri, C.M., Busso, M., Gallino, R., and Gratton, R. 1993, *A&A*, 272, 421
- Minniti, D., Zijlstra A.A., 1997, *AJ*, 114, 147 = MZ97
- Mirabel I.F., Lutz D., Maza J., 1991, *A&A*, 243, 367
- O'Brian T.R., Wickliffe M.E., Lawler J.E., Whaling W., Brault J.W., 1991, *J. Opt. Soc. Am.*, B8, 1185
- Pagal B.E.J., 1997, *Nucleosynthesis and Chemical Evolution of Galaxies*, CUP, pp.236
- Pagal B.E.J., Tautvaisienė G., 1998, *MNRAS*, 299, 535

- Peimbert M., 1993, *Rev. Mexicana Astron. Astrof.*, 27, 9
- Przybilla, N., 2002, Ph.D. thesis, Univ. München
- Przybilla, N., Butler K., Becker S.R., Kudritzki R.P., 2001a, *A&A*, 369, 1009
- Przybilla, N., Butler K., 2001b, *A&A*, 379, 955
- Przybilla, N., Butler K., Becker S.R., Kudritzki R.P., Venn K.A., 2000, *A&A*, 359, 1085
- Putman M., et al., 2002, *AJ*, 123, 873
- Rejkuba M., Minniti D., Gregg M.D., Zijlstra A.A., Victoria Alonso M., Goudfrooij P., 2000, *AJ*, 120, 801
- Richer M.G., McCall M.L., 1995, *ApJ*, 445, 642
- Rolleston W.R.J., Trundle C., Dufton P.L., 2002, *A&A*, 396, 53
- Rolleston W.R.J., Venn K.A., Tolstoy E., Dufton P.L., 2003, *A&A*, 400, 21
- Sandage A., Carlson G., 1985, *AJ*, 90, 1464
- Schweizer F., 1978, in *Structure and Properties of Nearby Galaxies*, ed. E.M. Berkhuijsen & R. Wielebinski (Dordrecht: Reidel), 279
- Shetrone M.D., Côté P., Sargent W.L.W., 2001, *ApJ*, 548, 592
- Shetrone M.D., Venn K.A., Tolstoy E., Primas F., Hill V., Kaufer A., 2003, *AJ*, 125, 684
- Sigut T.A.A., Landstreet J.D., 1990, *MNRAS*, 247, 611
- Skillman E.D., Kennicutt R.C., Hodge P.W., 1989b, *ApJ*, 347, 875
- Skillman E.D., Terlevich, R., Melnick J., 1989a, *MNRAS*, 240, 563
- Sofia U.J., Cardelli J.A., Savage B.D., 1994, *ApJ*, 430, 650
- Taylor C.L., Klein U., 2001, *A&A*, 336, 811
- Taylor C.L., Brinks E., Grashuis R.M., Skillman E.D., 1995, *ApJS*, 99, 427
- Tinsley B., 1979, *ApJ*, 229, 1046
- Tolstoy E., Venn K.A., Shetrone M.D., Primas F., Hill V., Kaufer A., Szeifert T., 2003, *AJ*, 125, 707

- Trundle C., Dufton P.L., Lennon D.J., Smartt S.J., Urbaneja M.A., 2002, *A&A*, 395, 519
- van den Bergh, S., 1994, *AJ*, 107, 1328
- van den Bergh, S., 2000, *PASP*, 112, 529
- Venn, K.A., 1999, *ApJ*, 518, 405
- Venn, K.A., 1995a, *ApJ*, 449, 839
- Venn, K.A., 1995b, *ApJS*, 99, 659
- Venn, K.A., Smartt S.J., Lennon D.J., Dufton P.L., *A&A*, 334, 987
- Venn, K.A., McCarthy J.K., Lennon D.J., Przybilla N., Kudritzki R.P., Lemke M., 2000, *ApJ*, 541, 610
- Venn, K.A., Lennon D.J., Kaufer A., McCarthy J.K., Przybilla N., Kudritzki R.P., Lemke M., Skillman E.D., Smartt S.J., 2001, *ApJ*, 547, 776
- Welty D.E., Lauroesch J.T., Blades C., Hobbs, L.M., York D.G., 2001, *ApJ*, 554, 75
- Welty D.E., Lauroesch J.T., Blades C., Hobbs, L.M., York D.G., 1997, *ApJ*, 489, 672
- Whiting A.B., Hau G.K.T., Irwin M., 2002 *ApJS*, 141, 123
- Whiting A.B., Hau G.K.T., Irwin M., 1999, *AJ*, 118, 2767
- Wiese W.L., Martin G.A., 1980 in *Wavelengths and Transition Probabilities for Atoms and Atomic Ions*, ed. J. Reader (Natl. Stand. Ref. Data Ser., 68) (Washington: Natl. Bur. Stand.), 22
- Zijlstra A.A., Minniti D., 1999, *AJ*, 117, 1743
- Zhu Q., Bridges J.M., Hahn T., Wiese W.L., 1989 *Phys. Rev. A*, 40, 3721

Table 1. WLM VLT UVES Observations

Obj	Date	UT Begin	$\lambda_c$ Å	Exptime sec	Airmass	Seeing arcsec	
WLM31	20Aug2000	04:33	390+564	3600	1.19	0.89	
		05:34	390+564	3600	1.06	0.73	
		06:35	390+564	3600	1.01	0.87	
	21Aug2000	02:44	390+564	3600	1.82	0.78	
WLM15	21Aug2000	04:02	390+564	3600	1.29	1.60	
		06:14	390+564	2470	1.02	1.03	
		07:06	390+564	2470	1.02	0.68	
			08:09	390+840	3600	1.08	0.97
	22Aug2000	02:52	390+840	3600	1.70	0.70	
03:53		390+840	3600	1.31	0.81		

Note. — Dichroic, 2x2 binning, and 1.0" slit throughout.

Table 2. WLM Sample

Obj	V <sup>1</sup>	(B-V) <sup>1</sup>	RV <sub>helio</sub> km/s	SpTy	Comment
WLM-31	18.42	0.24	−117	A5 Ib	VLT UVES
WLM-15	18.13	0.01	−101	A5 Ib	VLT UVES
WLM-35	18.06	−0.05	−133	early-B	VLT UVES
WLM-10	18.20	−0.06		late-B	WHT ISIS <sup>2</sup>
WLM-30	18.13	−0.30		early-B	ESO 3.6m EFOSC <sup>2</sup>
WLM-61	17.23	0.56		foreground	ESO 3.6m EFOSC <sup>2</sup>

<sup>1</sup>From Sandage & Carlson (1985).

<sup>2</sup>Lower resolution spectroscopy by D.J. Lennon and S.J. Smartt, including ESO 3.6m EFOSC (1989, resolution  $\sim 100 \text{ km s}^{-1}$ ) and WHT ISIS (July 2000, resolution  $\sim 50 \text{ km s}^{-1}$ ).

Table 3. Atomic Line Data and LTE Line Abundances

$\lambda$	$\chi$ (eV)	log gf	REF	WLM15 EQW	WLM15 log(X/H)	WLM31 EQW	WLM31 scaled	WLM31 log(X/H)
<b>N I<sub>NLTE</sub></b>								
7442.30	10.33	-0.39	zhu	45:+syn	7.50	...	...	...
7468.31	10.34	-0.19	zhu	60:+syn	7.50	...	...	...
<b>O I</b>								
6155.99	10.74	-0.67	op	syn	8.6	...	...	...
6156.78	10.74	-0.45	op	syn	8.6	...	...	...
6158.19	10.74	-0.31	op	60+syn	8.58	...	...	...
<b>Na I</b>								
5889.95	0.00	0.11	wm A	135+syn	6.03	...	...	...
5895.92	0.00	-0.19	wm A	91+syn	5.83	...	...	...
<b>Mg I<sub>NLTE</sub></b>								
3829.36	2.71	-0.21	fw B	125+syn	6.94	135	138	6.88
4702.99	4.35	-0.37	fw C	35+syn	7.02	30	36	6.96
5167.32	2.71	-0.86	fw B	80+syn	6.94	80	110	7.18
5172.68	2.71	-0.38	fw B	135+syn	7.01	93	127	6.86
5183.60	2.72	-0.16	fw B	150+syn	6.95	130	178	...
<b>Mg II<sub>NLTE</sub></b>								
3848.21	8.86	-1.56	fw C	21+syn	6.91	25	25	6.98
4390.57	10.00	-0.50	fw D	38+syn	6.90	...	...	...
7896.37	10.00	0.65	fw C+	110+syn	7.01	...	...	...
<b>Si I</b>								
3905.52	1.91	-1.09	fw C	99	6.95	90	92	6.74
<b>Si II</b>								
3853.66	6.86	-1.60	fw E	71	6.85	51	52	6.51
3856.02	6.86	-0.65	fw D+	142	6.91	140	143	6.64
3862.59	6.86	-0.90	fw D+	110	6.70	102	104	6.45
4130.89	9.84	0.46	fw C	58	6.39	85	91	6.74
5041.02	10.07	0.17	fw D+	56	7.01	37	48	6.80
5055.98	10.07	0.44	fw D+	45	6.54	27	35	6.29

Table 3—Continued

$\lambda$	$\chi$ (eV)	log gf	REF	WLM15 EQW	WLM15 log(X/H)	WLM31 EQW	WLM31 scaled	WLM31 log(X/H)
Sc II								
4314.08	0.62	-0.10	mfw D	96	2.45	80	90	2.27
4320.73	0.61	-0.21	fmw D-	84	2.42	104	117	2.60
4325.00	0.60	-0.44	mfw D	73	2.52	101	113	2.79
4374.46	0.62	-0.42	mfw D	83	2.62	77	88	2.56
4415.56	0.60	-0.64	k88	45	2.38	85	98	2.85
Ti II								
3932.02	1.13	-1.78	mfw D	81	4.69	63	64	4.42
4012.40	0.57	-1.61	mfw C	112	4.49	134	137	4.54
4025.13	0.61	-1.98	mfw D-	82	4.51	79	81	4.41
4028.34	1.89	-1.00	mfw D	94	4.59	120	122	4.72
4053.81	1.89	-1.21	mfw D	83	4.66	98	101	4.72
4161.54	1.08	-2.36	mfw D	35	4.62	62	66	4.96
4163.63	2.59	-0.40	mfw D	117	4.76	120	127	4.63
4171.92	2.60	-0.56	mfw D	112	4.86	108	114	4.67
4287.87	1.08	-2.02	mfw D-	86	4.89	75	84	4.77
4301.92	1.16	-1.16	mfw D-	109	4.37	118	133	4.40
4312.86	1.18	-1.16	mfw D-	148	4.96	140	158	4.67
4316.80	2.05	-1.42	mfw D-	60	4.68	33	37	4.35
4320.96	1.16	-1.87	fmw D-	66	4.57	107	120	4.99
4330.25	2.05	-1.52	mfw D	30	4.36	42	48	4.59
4350.83	2.06	-1.40	mfw D	29	4.23	30	34	4.29
4367.66	2.59	-1.27	mfw D-	67	4.99	64	73	4.98
4374.82	2.06	-1.29	mfw D	55	4.49	...	...	...
4386.84	2.60	-1.26	mfw D-	57	4.87	35	40	4.61
4394.05	1.22	-1.59	mfw D-	65	4.32	68	78	4.38
4395.85	1.24	-2.17	fmw D-	56	4.80	...	...	...
4399.77	1.24	-1.27	fmw D-	115	4.60	141	162	4.85
4407.68	1.22	-2.47	fmw D-	21	4.53	34	39	4.83
4417.72	1.15	-1.43	mfw D-	104	4.55	140	161	4.93
4418.33	1.24	-2.45	mfw D-	32	4.75	47	54	5.01
4441.73	1.18	-2.41	mfw D-	44	4.84	...	...	...
4450.48	1.08	-1.45	mfw D-	84	4.28	135	157	4.85
4464.45	1.16	-2.08	mfw D-	65	4.76	82	94	4.96
4501.27	1.12	-0.75	mfw D-	150	4.49	157	181	...
4779.99	2.05	-1.37	fmw D-	70	4.71	59	73	4.67

Table 3—Continued

$\lambda$	$\chi$ (eV)	log gf	REF	WLM15 EQW	WLM15 log(X/H)	WLM31 EQW	WLM31 scaled	WLM31 log(X/H)
4805.09	2.06	-1.12	fmw D-	95	4.75	93	114	4.79
4874.01	3.09	-0.79	mfw D	59	4.73	60	74	4.83
4911.19	3.12	-0.33	mfw D	52	4.21	48	60	4.25
5013.68	1.58	-1.94	k88	32	4.44	20	26	4.32
5129.15	1.89	-1.40	mfw D-	76	4.67	39	53	4.37
5154.07	1.57	-1.92	mfw D-	46	4.61	...	...	...
5185.91	1.89	-1.35	mfw D	42	4.22	...	...	...
5188.68	1.58	-1.22	mfw D-	116	4.72	82	112	4.51
5226.54	1.57	-1.29	mfw D-	87	4.45	...	...	...
5381.02	1.57	-2.08	mfw D	28	4.49	...	...	...
5418.75	1.58	-2.00	k88	27	4.39	...	...	...
Cr I								
4254.33	0.00	-0.11	mfw B	44	5.20	67	74	5.46
4274.80	0.00	-0.23	mfw B	57	5.49	60	66	5.50
5206.04	0.94	0.02	mfw B	30	5.45	...	...	...
5208.42	0.94	0.16	mfw B	35	5.40	...	...	...
Cr II								
4111.00	3.74	-1.92	k88	39	5.20	42	44	5.24
4145.78	5.32	-1.16	k88	27	5.28	...	...	...
4224.86	5.33	-1.06	k88	30	5.24	...	...	...
4242.36	3.87	-1.17	sl	101	5.32	84	92	5.07
4252.63	3.86	-2.02	k88	30	5.23	33	36	5.30
4261.91	3.86	-1.53	k88	69	5.28	97	107	5.56
4275.57	3.86	-1.71	k88	60	5.35	53	58	5.27
4284.19	3.85	-1.86	k88	39	5.21	50	55	5.38
4634.10	4.07	-1.24	mfw D	77	5.20	...	...	...
4824.13	3.87	-1.22	mfw D	113	5.48	110	136	5.51
4836.22	3.86	-2.25	mfw D	36	5.54	...	...	...
4848.24	3.86	-1.14	mfw D	90	5.10	99	123	5.30
4876.41	3.86	-1.46	mfw D	85	5.36	78	98	5.38
4884.61	3.86	-2.13	k88	35	5.40	...	...	...
5237.33	4.06	-1.16	mfw D	79	5.13	...	...	...
5274.96	4.05	-1.29	k88	57	5.00	...	...	...
5334.87	4.07	-1.56	k88	60	5.31	...	...	...

Table 3—Continued

$\lambda$	$\chi$ (eV)	log gf	REF	WLM15 EQW	WLM15 log(X/H)	WLM31 EQW	WLM31 scaled	WLM31 log(X/H)
Fe I								
3787.88	1.01	-0.84	ob	60	6.80	...	...	...
3820.43	0.86	0.16	ob	158	7.22	...	...	...
3825.88	0.91	-0.03	ob	145	7.19	...	...	...
3859.91	0.00	-0.71	fmw B+	144	7.18	166	169	...
3895.66	0.11	-1.67	fmw B+	71	7.11	89	91	7.19
3920.26	0.12	-1.75	fmw B+	55	7.00	80	82	7.19
3922.91	0.05	-1.65	fmw B+	76	7.10	105	107	7.27
3927.92	0.11	-1.59	fmw C	56	6.84	86	88	7.08
3930.30	0.09	-1.59	fmw C	91	7.25	91	93	7.11
4005.24	1.56	-0.61	fmw B+	58	6.90	96	98	7.20
4021.87	2.76	-0.66	fmw C+	34	7.44	43	44	7.53
4045.81	1.48	0.28	ob	130	6.93	138	142	...
4071.74	1.61	-0.02	fmw B+	88	6.70	106	111	6.76
4132.06	1.61	-0.67	ob	67	7.08	98	105	7.34
4143.87	1.56	-0.51	ob	74	6.97	76	81	6.92
4187.80	2.43	-0.55	fmw B+	45	7.25	36	39	7.11
4198.30	2.40	-0.72	fmw B+	30	7.17	25	27	7.06
4199.10	3.05	0.25	fmw C	47	6.91	53	58	6.96
4202.03	1.48	-0.71	fmw B+	53	6.85	65	71	6.96
4233.60	2.48	-0.60	fmw B+	57	7.49	60	66	7.50
4235.94	2.43	-0.34	fmw B+	50	7.10	60	66	7.20
4250.12	2.47	-0.40	fmw B+	37	7.01	60	66	7.29
4250.79	1.56	-0.72	fmw D-	45	6.81	84	93	7.23
4260.47	2.40	-0.02	fmw D	98	7.35	78	87	7.06
4271.15	2.45	-0.35	fmw B+	45	7.06	69	77	7.33
4271.76	1.48	-0.16	fwm B+	101	6.88	158	175	...
4282.40	2.18	-0.82	fmw C+	35	7.19	39	43	7.25
4325.76	1.61	0.01	ob	120	7.06	109	123	6.80
4383.54	1.48	0.21	ob	110	6.62	174	198	...
4415.12	1.61	-0.61	fmw B+	83	7.18	77	89	7.10
4459.12	2.18	-1.28	fmw B+	23	7.41	...	...	...
4466.55	2.83	-0.60	fmw C+	26	7.24	...	...	...
4476.02	2.85	-0.73	k88	32	7.50	...	...	...
4494.56	2.20	-1.14	fmw B+	30	7.42	25	29	7.36
4871.32	2.86	-0.42	k88	35	7.23	58	72	7.60
4872.14	2.88	-0.62	k88	19	7.12	30	37	7.42

Table 3—Continued

$\lambda$	$\chi$ (eV)	log gf	REF	WLM15 EQW	WLM15 log(X/H)	WLM31 EQW	WLM31 scaled	WLM31 log(X/H)
4890.75	2.88	-0.42	fmw C+	30	7.15	...	...	...
4891.50	2.85	-0.11	ob	50	7.12	50	63	7.19
4919.00	2.87	-0.37	fmw C+	37	7.21	48	60	7.44
4920.50	2.83	0.06	fmw C+	70	7.18	80	100	7.36
4957.60	2.84	-0.49	fmw D	50	7.49	...	...	...
5192.34	3.00	-0.52	k88	23	7.19	...	...	...
5364.86	4.45	0.22	fmw D	22	7.42	...	...	...
5371.49	0.96	-1.64	wm B+	22	6.84	...	...	...
5383.37	4.31	0.50	fmw C+	50	7.51	...	...	...
5405.77	0.99	-1.84	wm B+	28	7.19	...	...	...
5429.70	0.96	-1.88	wm B+	25	7.15	...	...	...
Fe II								
3783.35	2.27	-3.16	k88	95	6.87	120	122	6.97
3945.21	1.70	-4.25	k88	55	7.03	58	59	7.02
4057.46	7.27	-1.55	k88	27	7.42	...	...	...
4128.75	2.58	-3.76	fmw D	70	7.31	57	60	7.12
4258.15	2.70	-3.40	fmw D	68	7.02	107	117	7.38
4273.32	2.70	-3.34	fmw D	75	7.05	81	90	7.07
4296.57	2.70	-3.10	mfw D	97	7.05	115	128	7.19
4303.17	2.70	-2.49	fmw D	149	7.22	...	...	...
4354.34	7.65	-1.40	k88	22	7.41	...	...	...
4369.41	2.78	-3.66	fmw D	45	7.01	83	95	7.49
4385.38	2.78	-2.57	fmw D	140	7.19	...	...	...
4472.92	2.84	-3.43	fmw D	75	7.19	50	59	6.94
4489.18	2.83	-2.97	fmw D	75	6.72	114	133	7.18
4491.40	2.86	-2.69	fmw C	131	7.20	127	148	7.07
4629.34	2.81	-2.38	fw D	140	6.98	...	...	...
4635.32	5.96	-1.65	fmw D-	40	7.00	...	...	...
4663.71	2.89	-4.27	k88	30	7.45	...	...	...
4666.75	2.83	-3.33	fmw D	74	7.06	64	78	7.02
4731.45	2.89	-3.37	fmw D	67	7.06	74	91	7.22
4993.36	2.81	-3.65	fmw E	47	7.03	...	...	...
5197.57	3.23	-2.10	fmw C	135	6.88	122	167	6.91
5234.62	3.22	-2.05	fmw C	129	6.74	...	...	...
5264.81	3.23	-3.19	fmw D	59	7.01	...	...	...
5284.10	2.89	-3.19	fmw D	67	6.87	...	...	...

Table 3—Continued

$\lambda$	$\chi$ (eV)	log gf	REF	WLM15 EQW	WLM15 log(X/H)	WLM31 EQW	WLM31 scaled	WLM31 log(X/H)
5337.73	3.23	-3.31	k88	35	6.80	...	...	...
5362.86	3.20	-2.74	k88	105	7.09	...	...	...
5425.25	3.20	-3.36	fmw D	53	7.09	...	...	...
5534.85	3.24	-2.92	fmw D	85	7.06	...	...	...
6147.74	3.89	-2.46	fmwy D	48	6.62	...	...	...
6149.24	3.89	-2.77	fmw D	55	7.02	...	...	...
6238.38	3.89	-2.48	k88	87	7.13	...	...	...
6247.56	3.89	-2.36	fmw D	68	6.78	...	...	...
6416.91	3.89	-2.70	fmw D	70	7.15	...	...	...
6456.38	3.90	-2.16	fmw D	120	7.24	...	...	...
7462.41	3.89	-2.73	k88	90	7.48	...	...	...
Sr II								
4077.71	0.00	0.17	k88	62	1.19	116	121	1.67
Zr II								
4149.22	0.80	-0.03	k88	54	2.30	70	75	2.46
Ba II								
4934.08	0.00	-0.15	k88	30:	1.66	50	63	2.03

References. — Transition Probability References: fw = Fuhr & Wiese (1998); fmw = Fuhr, Martin, & Wiese (1988); fmwy = Fuhr et al. (1981); k88 = Kurucz (1988); mfw = Martin, Fuhr, & Wiese (1988); ob = O’Brian et al. (1991); op = Opacity Project (Hibbert et al. 1991); sl = Sigut & Landstreet (1990); wm = Wiese & Martin (1980); zhu = Zhu et al. (1989).

Table 4. Atmospheric Analysis

	Solar	WLM-15	WLM-31
$T_{\text{eff}}$		$8300 \pm 200$	$8300 \pm 300$
$\log g$		$1.6 \pm 0.1$	$1.65 \pm 0.1$
$\xi$		$3 \pm 1$	$4 \pm 1$
$\log(L/L_{\odot})^{\text{a}}$		$4.55 \pm 0.20$	...
$R/R_{\odot}^{\text{a}}$		$91 \pm 20$	...
Sp. Ty.		A5 Ib	A5 Ib
N I NLTE	7.80	$7.50 \text{ (syn)} \pm 0.04$	...
O I NLTE	8.66	$8.45 \text{ (syn)} \pm 0.05$	...
Na I	6.32	$5.93 \pm 0.14 \text{ (2)} \pm 0.30$	...
Mg II NLTE	7.58	$6.94 \pm 0.06 \text{ (3)} \pm 0.08$	$6.97 \text{ (1)} \pm 0.03$
Mg I NLTE	7.58	$6.97 \pm 0.04 \text{ (5)} \pm 0.26$	$6.96 \pm 0.15 \text{ (4)} \pm 0.43$
Si II	7.56	$6.73 \pm 0.23 \text{ (6)} \pm 0.14$	$6.57 \pm 0.19 \text{ (6)} \pm 0.15$
Si I	7.56	$6.95 \text{ (1)} \pm 0.31$	$6.74 \text{ (1)} \pm 0.42$
Ti II	4.94	$4.60 \pm 0.21 \text{ (40)} \pm 0.20$	$4.65 \pm 0.24 \text{ (31)} \pm 0.26$
Sc II	3.10	$2.48 \pm 0.09 \text{ (5)} \pm 0.22$	$2.62 \pm 0.23 \text{ (5)} \pm 0.34$
Cr II	5.69	$5.27 \pm 0.14 \text{ (17)} \pm 0.09$	$5.33 \pm 0.15 \text{ (9)} \pm 0.15$
Cr I	5.69	$5.38 \pm 0.13 \text{ (4)} \pm 0.29$	$5.48 \pm 0.03 \text{ (2)} \pm 0.45$
Fe II	7.50	$7.06 \pm 0.21 \text{ (35)} \pm 0.16$	$7.12 \pm 0.17 \text{ (13)} \pm 0.19$
Fe I	7.50	$7.13 \pm 0.22 \text{ (47)} \pm 0.30$	$7.18 \pm 0.22 \text{ (30)} \pm 0.44$
Sr II	2.92	$1.21 \text{ (1)} \pm 0.34$	$1.67 \text{ (1)} \pm 0.50$
Zr II	2.61	$2.30 \text{ (1)} \pm 0.17$	$2.46 \text{ (1)} \pm 0.32$
Ba II	2.22	$1.66 \text{ (1)} \pm 0.35$	$2.03 \text{ (1)} \pm 0.50$

<sup>a</sup>The WLM-15 luminosity and radius are determined from the stellar atmospheric parameters and adopting  $M = 12 M_{\odot}$  from standard stellar evolution tracks, e.g., Lejeune & Schaerer (2001). We suggest that WLM-31 may have a slightly lower mass (see Section 3.2

Note. — Two uncertainties are shown for each elemental abundance, the line-to-line scatter (also shown are the number of lines used in the abundance), and an estimate of the systematic error in italics. The systematic errors are based on the uncertainties in the atmospheric parameters, tabulated in Table 5. Solar abundances are Grevesse & Sauval (1998), with the exception of N and O from Asplund (2003). Although

Table 5. Standard LTE Abundance Uncertainties

	WLM-15	WLM-15 <sup>1</sup>	WLM-15 <sup>1</sup>	WLM-15 <sup>2</sup>	WLM-31
	$\Delta T_{\text{eff}}$	$\Delta \log g$	$\Delta \xi$	Helium	$\Delta T_{\text{eff}}$
	=+200 K	=+0.1	=+1 km/s	Test	=+300 K
$\Delta \log(\text{NI}/\text{H})$	+0.03	−0.02	−0.02	+0.05	...
$\Delta \log(\text{OI}/\text{H})$	+0.02	0.00	−0.05	+0.04	...
$\Delta \log(\text{NaI}/\text{H})$	+0.25	−0.06	−0.14	+0.03	...
$\Delta \log(\text{MgII}/\text{H})$	0.00	0.00	−0.08	+0.03	+0.03
$\Delta \log(\text{MgI}/\text{H})$	+0.20	−0.06	−0.16	+0.01	+0.39
$\Delta \log(\text{SiII}/\text{H})$	−0.02	+0.01	−0.14	+0.04	−0.05
$\Delta \log(\text{SiI}/\text{H})$	+0.28	−0.06	−0.13	−0.02	+0.40
$\Delta \log(\text{TiII}/\text{H})$	+0.17	0.00	−0.10	−0.06	+0.24
$\Delta \log(\text{ScII}/\text{H})$	+0.21	−0.01	−0.08	−0.07	+0.33
$\Delta \log(\text{CrII}/\text{H})$	+0.06	0.00	−0.07	−0.04	+0.14
$\Delta \log(\text{CrI}/\text{H})$	+0.28	−0.06	−0.03	−0.02	+0.45
$\Delta \log(\text{FeII}/\text{H})$	+0.10	+0.01	−0.12	−0.03	+0.15
$\Delta \log(\text{FeI}/\text{H})$	+0.28	−0.06	−0.10	−0.02	+0.42
$\Delta \log(\text{SrII}/\text{H})$	+0.33	−0.04	−0.07	−0.06	+0.49
$\Delta \log(\text{ZrII}/\text{H})$	+0.16	−0.01	−0.05	−0.07	+0.32
$\Delta \log(\text{BaII}/\text{H})$	+0.34	−0.06	−0.02	−0.04	+0.50

<sup>1</sup>Uncertainties in gravity and microturbulence for WLM31 are similar to those listed here for WLM15.

<sup>2</sup>An ATLAS9 model atmosphere for WLM15 with 40% helium content has been adopted for this test. Increasing helium also required a change in gravity of  $\Delta \log g = -0.3$  to fit the Balmer lines. No other changes were made (i.e., to  $T_{\text{eff}}$  or  $\xi$ ).

Table 6. Differential Abundance Ratios (SMC)

	AV 392	WLM-15 – AV 392	AV 463	WLM-15 – AV 463
Teff	8500		8000	
log g	1.7		1.3	
$\xi$	3		4	
Sp.Ty.	A3 Ib		A7 Ib	
[FeII/H]	-0.69 (19)	+0.25	-0.60 (33)	+0.16
[OI/H]	-0.46 (1)	+0.25	-0.46 (2)	+0.25
[Ni <sub>NLTE</sub> /FeII]	...	...	0.00 (1)*	+0.14
[OI <sub>NLTE</sub> /FeII]	+0.23 (1)	0.00	+0.14 (2)	+0.09
[MgI <sub>NLTE</sub> /FeII]	-0.06 (4)	-0.11	+0.01 (3)	-0.18
[MgII <sub>NLTE</sub> /FeII]	-0.06 (1)*	-0.14	+0.10 (1)*	-0.30
[SiII/FeII]	+0.24 (2)*	-0.58	-0.10 (2)*	-0.29
[NaI/FeII]	... <sup>a</sup>	...	-0.15 (2)	+0.20
[TiII/FeII]	+0.23 (22)	-0.13	+0.14 (32)	-0.04
[ScII/FeII]	+0.01 (1)*	-0.19	... <sup>a</sup>	...
[CrII/FeII]	+0.09 (12)	-0.07	-0.09 (15)	+0.11
[SrII/FeII]	-0.83 (1)*	-0.66	-1.11 (1)*	-0.16
[ZrII/FeII]	...	...	-0.17 (1)*	+0.30
[BaII/FeII]	...	...	-0.06 (1)*	-0.06

\*When only a few lines are used in the abundance ( $\leq 3$ ) then only the lines in common in both analyses are compared.

<sup>a</sup>No lines in common.

Table 7. Differential Abundance Ratios (NGC6822 & Galactic)

	NGC6822-cc	WLM-15 – NGC6822-cc	HD34578	WLM-15 – HD34578
Teff	8500		8300	
log g	1.1		1.85	
$\xi$	6		4	
Sp.Ty.	A3 Ia		A5 II	
[FeII/H]	−0.40 (20)	−0.04	+0.04 (17)	−0.48
[OI/H]	−0.22 (2)*	+0.01	−0.08 (3) <sup>a</sup>	−0.13
[NI/FeII]	...	...	+0.06 (2)*	+0.08
[OI <sub>NLTE</sub> /FeII]	+0.18 (2)*	+0.05	−0.12 (3) <sup>a</sup>	+0.35
[MgI <sub>NLTE</sub> /FeII]	+0.12 (2)*	−0.28	−0.09 (1)*	−0.03
[MgII <sub>NLTE</sub> /FeII]	+0.16 (1)*	−0.40	... <sup>b</sup>	...
[SiII/FeII]	+0.21 (1)*	−0.11	... <sup>b</sup>	...
[TiII/FeII]	+0.01 (13)	+0.09	+0.26 (17)	−0.16
[ScII/FeII]	+0.29 (2)*	−0.60	... <sup>b</sup>	...
[CrII/FeII]	−0.07 (10)	+0.09	+0.08 (4)	−0.06

\*When only a few lines are used in the abundance ( $\leq 3$ ) then only the lines in common in both analyses are compared.

<sup>a</sup>NLTE correction of  $-0.15$  dex has been applied to the LTE oxygen abundance for HD34578 by Venn 1995b.

<sup>b</sup>No lines in common.

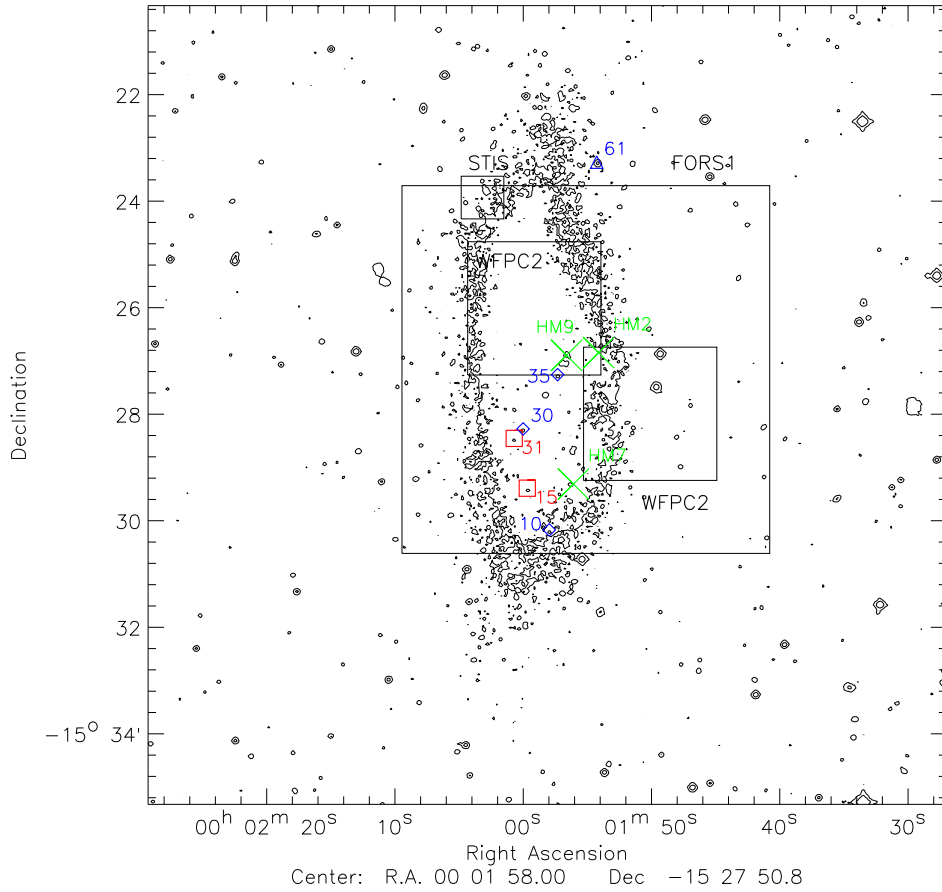


Fig. 1.— The WLM dwarf irregular galaxy. The two A-supergiants analysed in this paper are noted (in red), as well as other blue supergiants from the original target list (in blue) and listed in Table 2. The H II regions where oxygen abundances have been determined from the [O III]  $\lambda 4363$  line are marked (in green), and the fields of view for VLT-FORS1, HST-STIS, and HST-WFPC2 imaging are outlined.

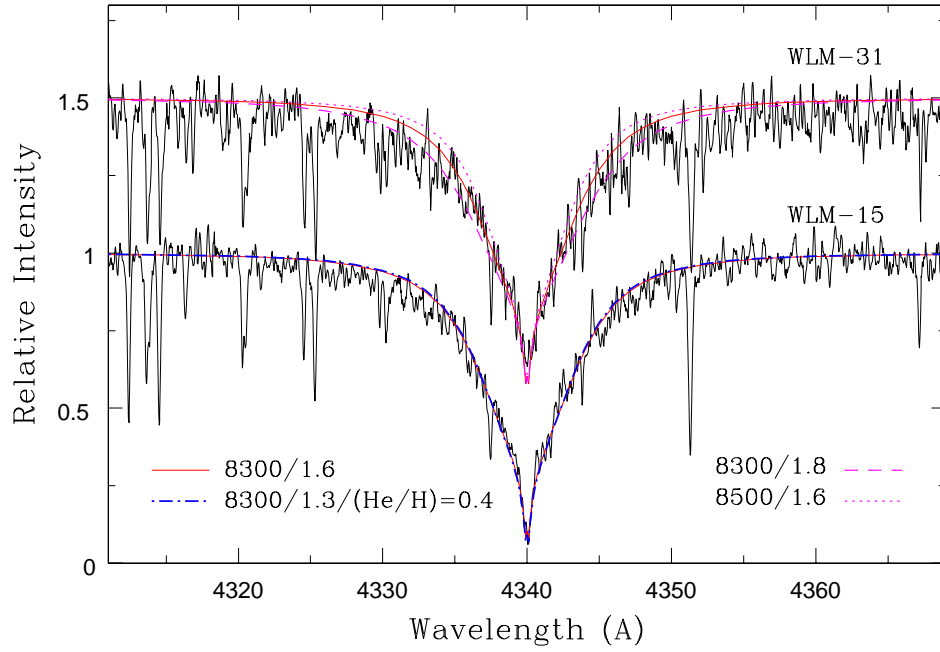


Fig. 2.—  $H\gamma$  profile for WLM-15 and WLM-31 and fits from different model atmospheres. The model with increased helium abundance and lower gravity is identical to the best fit model.

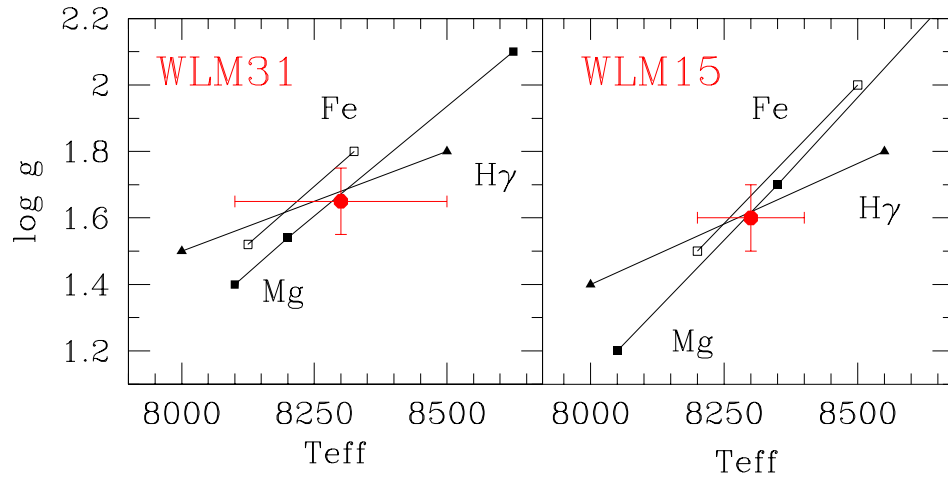


Fig. 3.— Atmospheric parameter selections for WLM-31 and WLM-15 (solid circles with errorbars).  $H\gamma$  fits (solid triangles), Mg I/Mg II (solid squares), and Fe I/Fe II (hollow squares) ionization equilibrium are used for both stars.

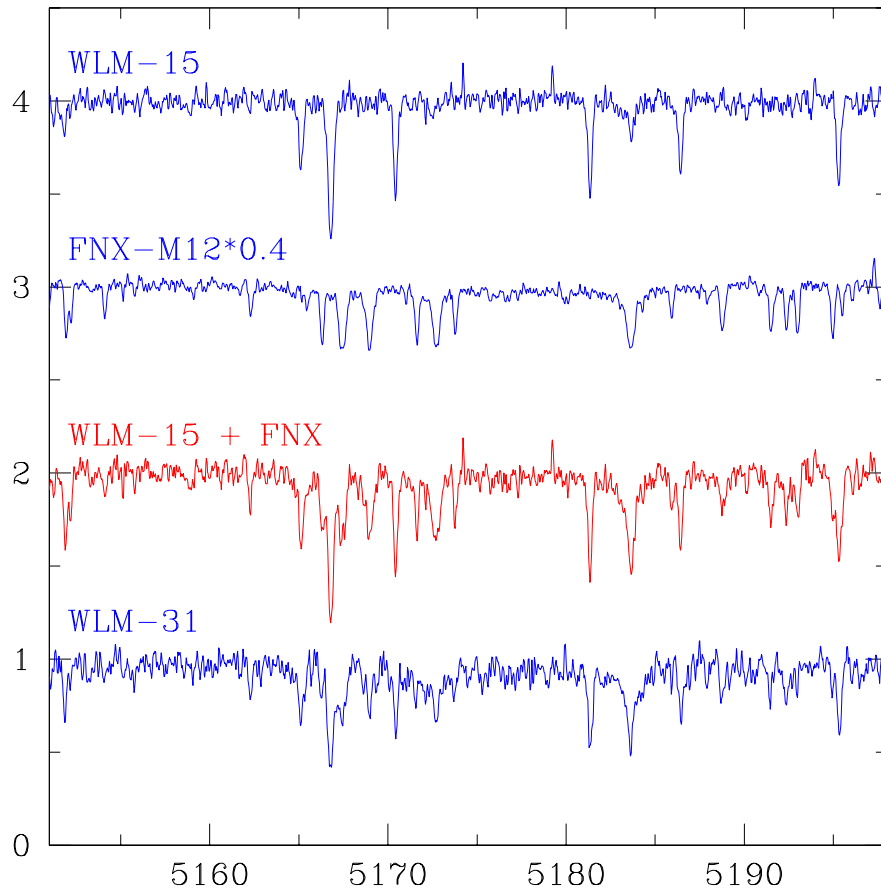


Fig. 4.— Spectrum of WLM-31 around the Mg b lines. The spectrum of WLM-15 is combined with that of a metal-poor red giant in Fornax (M12, Shetrone et al. 2003) scaled by 40%, to show that the combination is a very good match for the WLM-31 spectrum. Note that the Fornax red giant spectrum is only for illustration; in the text we discuss that the continuum scaling is independent of gravity near 4250 K, thus the contaminating star does not need to be a high luminosity red giant. The Fornax red giant has been corrected to have zero radial velocity, whereas the spectra of WLM-31 and WLM-15 have not been corrected for this illustration. The contribution of the red giant to the WLM-31 spectrum drop off at bluer wavelengths becoming negligible near 4000 Å (see text).

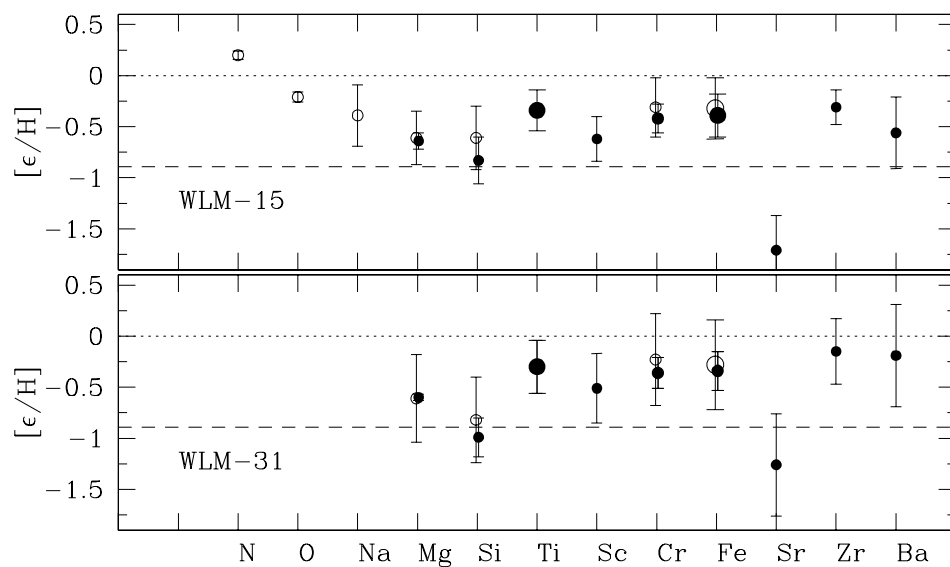


Fig. 5.— Elemental abundances for WLM-15 (top) and WLM-31 (bottom) relative to solar (dotted line) and to the nebular oxygen underabundance (dashed line). Surprisingly these two stars appear more metal-rich than the H II regions in WLM. Two errorbars are shown for each point: thick line for the line-to-line scatter and thin line for the systematic uncertainties (see text and Table 4). The largest data points include  $\geq 30$  line abundances, and the smallest include  $\leq 10$ .

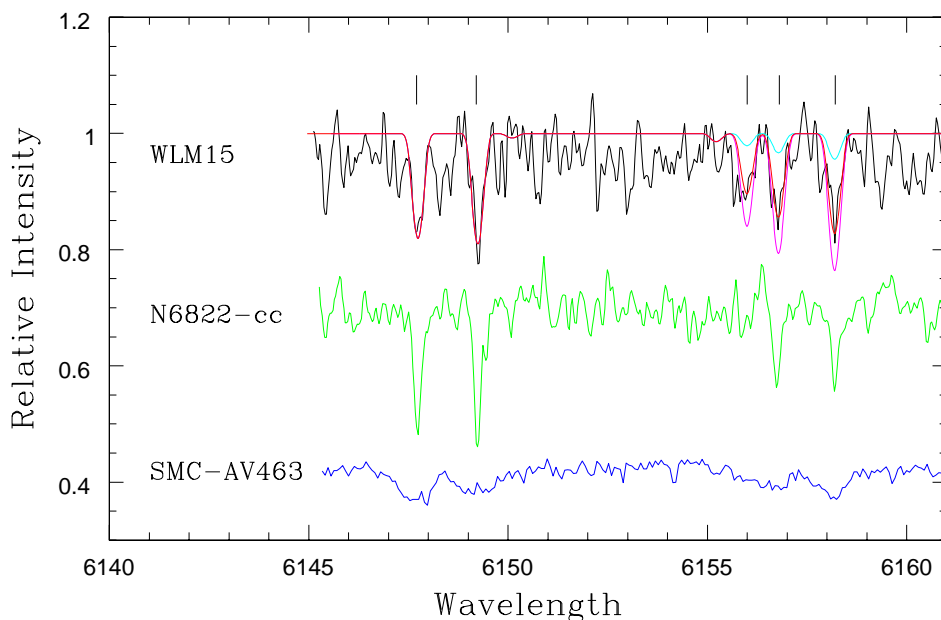


Fig. 6.— O I 6150 spectrum synthesis for WLM-15. Three oxygen abundances are shown;  $12+\log(\text{O}/\text{H}) = 8.6$  (best fit),  $= 8.9$  (too strong), and  $= 7.77$  (the nebular oxygen abundance). These are the LTE values; NLTE correction is  $-0.15$  from Przybilla et al. (2000). The oxygen feature is clearly well defined, and not reproduced by the low nebular value. Iron abundances for  $\lambda 6147$  and  $\lambda 6149$  line syntheses are those from the equivalent widths analysis (Table 3). Spectra of two comparison stars are shown; from model atmospheres analysis, the oxygen abundance is the same in WLM-15 and NGC6822-cc, while that for SMC-AV463 is 0.2 dex lower (see text).

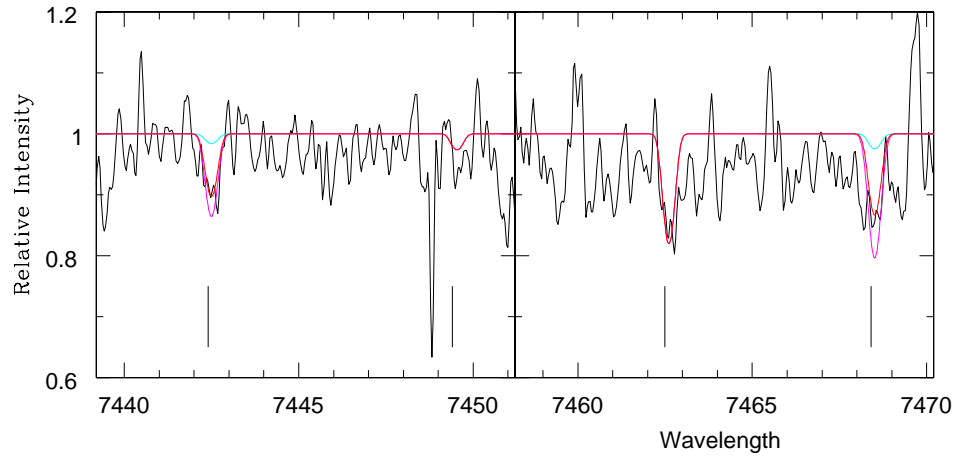


Fig. 7.— N I 7440 spectrum synthesis for WLM-15. Three nitrogen abundances are shown (NLTE);  $12+\log(\text{N}/\text{H}) = 7.5$  (best fit, red line),  $= 7.8$  (too strong, blue line),  $= 6.46$  (the mean nebular abundance from HM95, green line). The iron abundance for  $\lambda 7462$  in the synthesis is from the value found from its equivalent width analysis (the  $\lambda 7449$  iron line is also marked, but not used).

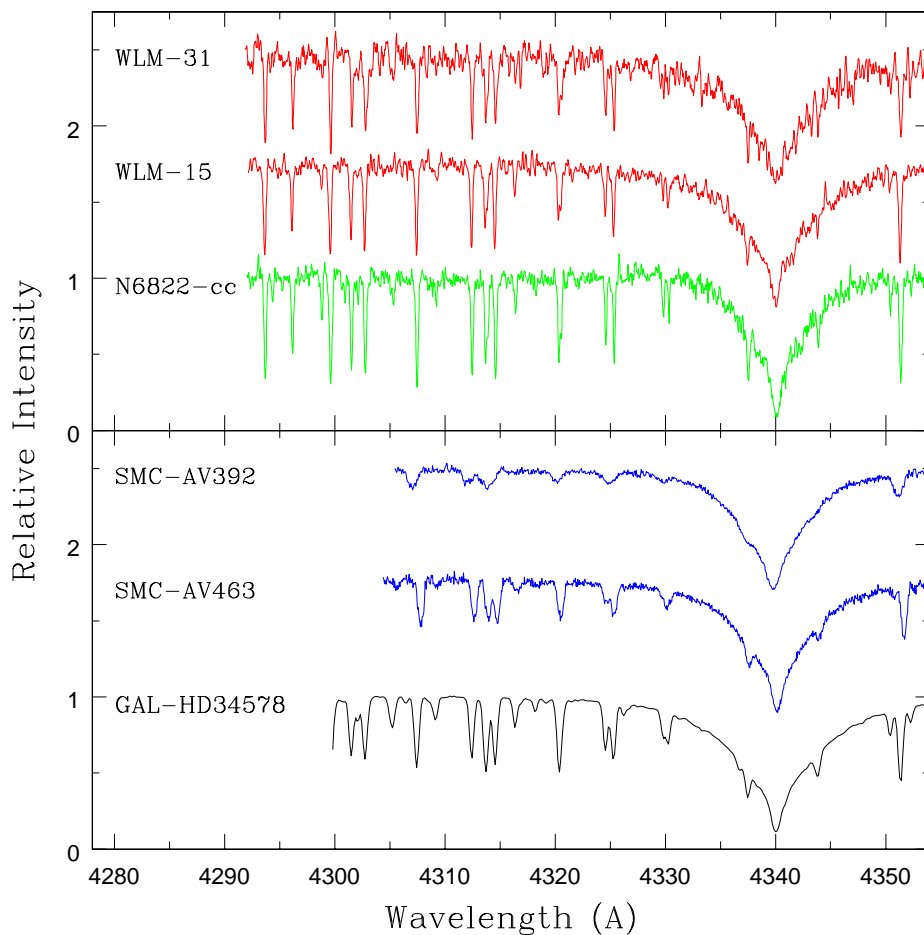


Fig. 8.— Spectra of iron-group lines around  $H\gamma$  in the WLM stars and comparison stars with very similar atmospheric parameters (see Tables 6 and 7). In the top panel, the similarities between NGC6822-cc and the two WLM stars are striking; the metal lines are nearly identical. In the lower panel, the higher broadening of the SMC and Galactic comparison stars make a direct comparison of the metal lines much more difficult. It is obvious that the SMC stars are more metal-poor than the Galactic star, but detailed model atmospheres analyses are needed to find that NGC6822-cc and the WLM stars have slightly higher metallicities than the SMC.

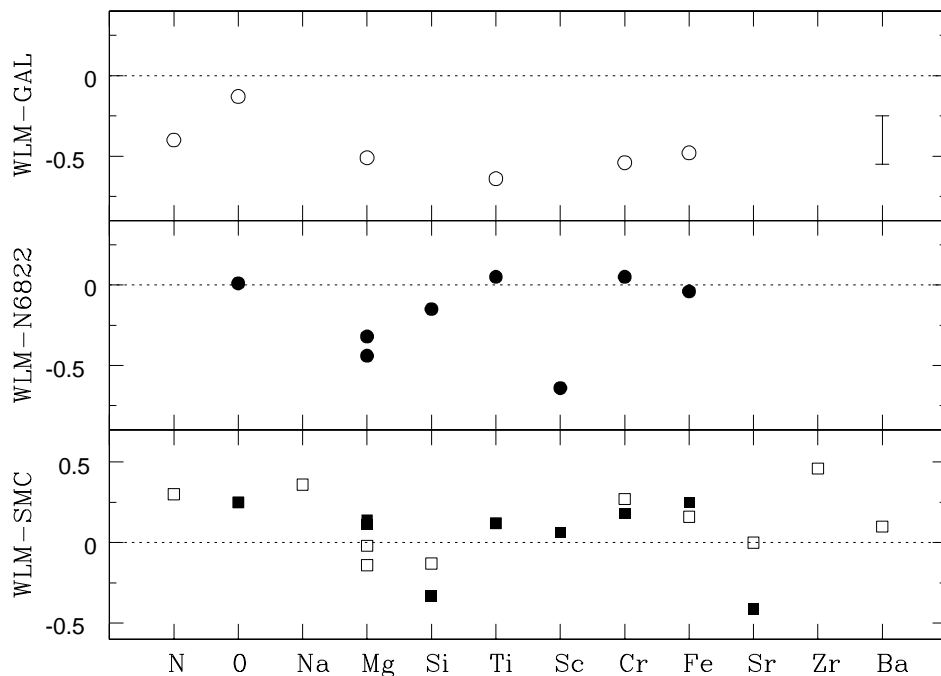


Fig. 9.— Differential abundances from Table 6 and 7, with the typical uncertainty shown in the top panel. Top panel shows that WLM-15 is more metal-poor than the Galactic comparison star HD 34578. Middle panel shows that WLM-15 is comparable to NGC6822-cc, except Mg seems lower; Sc is more uncertain in NGC6822-cc (see text). Lower panel shows that WLM-15 is generally more metal-rich than two SMC stars (AV392, filled squares; AV463, hollow squares), except Mg may be lower; Si and Sr are more uncertain in the SMC stars themselves (see text). The  $[O/Fe]$  ratios are similar in all stars, except when compared to the Galactic standard.

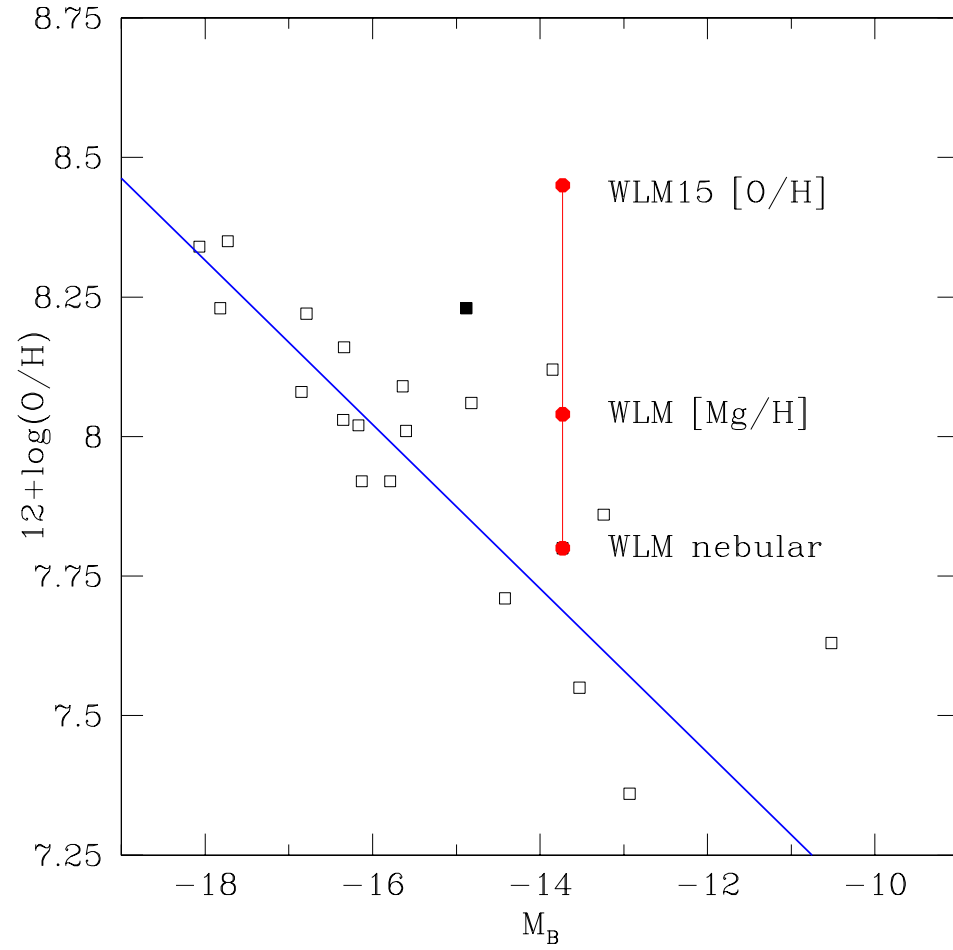


Fig. 10.— The metallicity-luminosity relationship for dwarf irregular galaxies from Richer & McCall (1995). Using the same  $M_B$  for WLM, the stellar oxygen abundance from WLM-15 is shown, as well as the location of the mean  $[\text{Mg}/\text{H}]$  abundance from both of the WLM stars. NGC 6822 is also noted (*solid square*).